CLASSIFICATION cancelled 8-25-47
RESEARCH & DEVEL. SUBOFFICE
J.P.L.

A CORRELATION OF HIGH SPEED DRAG DATA

Thesis by

Rudolph Hensel, 1st Lt. A.C.

Harry J. Heimer, 1st Lt. A.C.

In Partial Fulfillment of the Requirements for the Degree
of Aeronautical Engineer

California Institute of Technology
Pasadena, California

September 15, 1944

CLASSIFICATION cancelled 8-25-47
RESEARCH & DEVEL. SUBOFFICE
J.P.L.

CLASSIFICATION cancelled

Acknowledgements

The authors wish to express their thanks and appreciation to the following:

Dr. Hsue-shen Tsien, Dr. Clark B. Millikan and Lester Lees for many helpful suggestions offered throughout this investigation.

North American Aviation, Douglas Aircraft Company, Northrop Aircraft, and Lockheed Aircraft Corporation for their cooperation in allowing the authors the use of their libraries.

Colonel W. H. Joiner, and Major W. A. Bennett for their help in obtaining the necessary reports and data from the N.A.C.A.

The National Advisory Committee for Aeronautics for their cooperation in furnishing the necessary reports and data.

CLASSIFICATION cancelled

CONFIDENTIAL
CLASSIFICATION cancelled

A CORRELATION OF HIGH SPEED DRAG DATA

by

Harry J. Heimer, 1st Lt. A.C.

Rudolph W. Hensel, 1st Lt. A.C.

In fulfillment of Article 1(a) par. 2
of Supplemental Agreement No. 1 (S-4843)
to Contract No. W 33-038 ac - 1717(11592)

Galcit Project No. 11

Approved by: Clark B. Millikan

Th. von Karman
Director, Guggenheim
Aeronautical Laboratory

Copy No.____

California Institute of Technology

September 15, 1944

CLASSIFICATION cancelled
CONFIDENTIAL

CONFIDENTIAL
CLASSIFICATION cancelled

Table of Contents

I	Summary	1
II	Introduction	2
III	Blocking Effect	5
IV	The Determination of Wing Critical Mach Numbers	20
V	Results	31
VI	Conclusions	35
VII	Recommendations	37
VIII	References	38
IX	Figures	41
Appendix I		70
Appendix II		91

CLASSIFICATION cancelled

I Summary

In fulfillment of the purpose of this investigation, a method of estimating the drag of an airplane at high Mach numbers has been derived. Two sets of curves, one for airplanes having conventional wing sections and the other for those having low drag sections, were drawn to show the percentage increase in total drag with the ratio of free stream Mach number to critical Mach number of the wing.

A method for computation of the blocking correction is presented and applied, resulting in good agreement between the wind tunnel and flight tests. Wind tunnel data corrected for the blocking effect were chiefly used to deduce the conclusions, but they were supplemented by all the flight test results available.

CLASSIFICATION cancelled

II Introduction

In the past few years airplanes have reached the speed where the influence of compressibility has become a problem to the aeronautical engineer. One of these problems is the rapid increase in drag at high Mach numbers. When designing high speed airplanes this increase in drag becomes extremely important in estimating the terminal velocity and the level flight high speed. Wind tunnels have been built and are being built to help evaluate these high speed drags, but it is also necessary to be able to estimate the drag of a new airplane in the preliminary design stage before a wind tunnel model is constructed. To facilitate this, some type of general drag relation from which one may estimate the increase in drag with Mach number for any airplane is necessary. Empirical relations of this nature have been found and are included in this report.

The wind tunnel data used in deriving these generalized curves were obtained exclusively from the N.A.C.A. Sixteen Foot Wind Tunnel at the Ames Aeronautical Laboratory. This limitation was necessary because this is the only high speed wind tunnel in which complete, strut supported models have been tested. Results from tunnels using the wing tip support method were not used because it was felt that they could not be compared directly with flight conditions. These data were supplemented by all the flight test results available to the authors.

The wind tunnel results were all corrected for blocking effect by a method described in this report in section III. When these corrections are applied the wind tunnel results agree closely with flight tests.

CLASSIFICATION cancelled

The corrections are good engineering approximations at speeds below the critical Mach number,* but become less accurate as the Mach number increases because of the assumption that the flow is everywhere subsonic, whereas actually the problem involves mixed flows. This is an unfortunate limitation, but it is the only reasonable condition under which the problem can be approximately solved.

Section IV contains a description of the methods used in determining the critical Mach numbers of the wings. In as many cases as possible, experimental results were used, but in the few cases when these were not available, theoretical values were resorted to.

A great many tests are being performed in an attempt to learn more about high speed effects. Wind tunnel results are being severely criticized at the present time because the wind tunnel walls add another boundary condition at high speed. Flight results should not be used as a standard either, since at the present time flight test technique is not sufficiently developed to accurately measure these high speed effects. Some of the difficulties encountered are: calibration of the pitot-static system at high altitudes and high Mach numbers, evaluation of time lag of the airspeed altimeter system when the pressures are changing rapidly, measurement of thrust, and measurement of varying pressures in pressure distribution surveys. Considering these problems, it is apparent that great care must be exercised to see that errors which are unimportant in low speed tests do not obscure the true results of high

---

* Critical Mach number is defined as that value of the free stream Mach number at which sonic velocity first occurs in the flow field under consideration.

speed testing. Wind tunnel testing has a definite place in obtaining results up to a Mach number of about .9, but between .9 and 1.1 serious difficulties are encountered which make its use somewhat impractical. In flight testing, it is obvious that data taken near a Mach number of 1.0, where nose shock waves are appearing or disappearing, are unreliable unless steady, unaccelerated flight can be maintained.

Ballistic data were not used in this investigation because the shape of the bodies tested did not conform closely enough to an airplane. These tests are also questionable near the sonic speed where they would be most useful.

CONFIDENTIAL
CLASSIFICATION cancelled

III Blocking Effect

A. Introduction

In the comparison of drag measurements made in the wind tunnel and in free flight, considerable discrepancy is found to exist at higher values of Mach number. The tunnel drags in general increase more rapidly and at consistently lower Mach numbers than is indicated by the measurements obtained in flight. This difference in results is largely attributed to an effect caused by the finite dimensions of the air stream and model supports used in wind tunnel testing. This phenomenon, which is known as "blocking", involves primarily an increase of effective velocity and hence Mach number over the measured value, M, at the model. In order to attain the desired purpose of determining a universal drag function by causing the free stream and model results to coincide, wind tunnel results will be corrected for this blocking effect by the following method.

B. The Thom Method

According to the present knowledge of the authors, the most complete and theoretically sound method for the calculation of blocking is that given by Dr. A. Thom of the Royal Aircraft Establishment at Farnborough, England in their Report No. 1891 dated November 1943. In three dimensions, he considers not only the "solid" blocking associated with the increase in speed caused by the presence of a model alone, but also the effect of the solid blocking of the support strut guards on the model and the contribution of the wakes of the model and

CONFIDENTIAL
CLASSIFICATION cancelled

front and rear strut guards. The corrections for the solid blocking and wakes of two-dimensional models are also given.

Standard incompressible fluid methods involving the replacement of the parts under consideration by hydrodynamical singularities were used. Knowing these singularities and their image systems which satisfy the boundary condition of no flow across the tunnel walls ($\frac{\partial \varphi}{\partial n} = 0$), it was possible to calculate the flow field at any point in the tunnel. An extension to the higher speeds of a compressible fluid was made by using an appropriate Mach number power factor based on the Prandtl-Glauert approximation.

Goldstein and Young[2] show that the form of the corrected velocity is:

$$U_c = U(1+\epsilon_c) \tag{1}$$
$$= U\left(1+\frac{\epsilon}{\beta^n}\right)$$

where:

U_c = corrected tunnel speed

U = uncorrected tunnel speed

ϵ = incompressible (low speed) blocking factor

ϵ_c = compressible (high speed) blocking factor

$\beta = \sqrt{1-M^2}$, M being the Mach number corresponding to U. However, in practice a mean value between M and the corrected Mach number, M_c, will be used.

n = 2, 3, 4 depending upon the part of the model under consideration and if the flow is two or three dimensional.

ϵ_c is the sum of the separate values obtained from the wake and solid blocking of the flow constituents (i.e. model wing and fuselage and strut guards). The very rapid rise of $\frac{1}{\beta^n}$ as M approaches 1.0 is seen in Figure 1 for n = 2, 3, and 4.

Thom has worked out the different solid and wake blocking corrections upon the basis of a rectangular tunnel and more particularly, the RAE 7 by 10 foot high speed tunnel.

The first of the solid blocking cases considered was that of a two dimensional wing. For this, the wing was replaced by an infinite line source near the leading edge and appropriate rows of infinite line sink distributions to give the desired airfoil shape. The top and bottom walls were replaced by similar infinite image rows of line sources and sinks which were included to satisfy the boundary condition. To obtain the induced velocity at the model, the primary image (wing) was removed and the effect of the images was calculated.

The next step, logically, was the extension to the finite span, three dimensional wing. The same general procedure as in the two dimensional case was used except that the wing and its images were now represented by a series of finite length lines of sources and sinks. Thom obtained the approximate result:

(2) $$\epsilon_c = \frac{1.2\, s\, c\, t}{(BH)^{\frac{3}{2}} \beta^3}$$

where: s = wing semi-span

c = chord

t = thickness

B = tunnel width

H = tunnel height

Next, a body of revolution was represented by point sources and sinks at the centers of the primary and image tunnel sections. The result for this case and previous ones may be put in a general form:

$$\epsilon_c = \frac{k \cdot \text{VOLUME}}{(BH)^{\frac{3}{2}} \beta^n} \tag{3}$$

The volume of a wing is about .65 to .70 x (2stc) and the volume of a streamlined body of revolution (l = length, d = diameter) is approximately .40 to .45 x ld^2. k is a constant which is listed in Table I along with the appropriate value of n.

Table I

Case	k	n
Three dimensional wing	.90	3
Two dimensional wing spanning width of tunnel	.74	3
Two dimensional wing spanning height of tunnel	.52	3
Streamlined solid	.96	4

Note: Numerical Values for Rectangular 7 x 10 Tunnel

The final solid blocking correction concerns the induced velocity at the model due to the presence of the front strut guards. Again, these guards are replaced by finite length lines of sources and sinks. However, since the velocity increment is desired at the model rather than at the body under consideration and because of the very close proximity of the guards to the model, it was only necessary to consider the guards themselves and their nearest images. A small factor was

added for the remaining images. The result is of the form:

(4) $$\epsilon_c = k \cdot \frac{tc}{\beta^3}$$

where t and c are the guard thickness and chord respectively. The constant k is a function of the strut guards height, the distance between them and the configuration of source-sink distributions used. k also varies along the model span, but the value at the model midpoint coincides closely with the mean value of k when the struts are a semi-span apart. (see figure 10, ref. 1). Hence, for any given strut guard condition it was only necessary to calculate k at the center of the tunnel in the vertical plane which includes the wing span.

The presence of a wake behind a body placed in a wind tunnel causes a decrease in effective cross sectional area, resulting in a speeding up of the mean flow in the test section. This phenomena is known as wake blocking. The wake was represented by a source at the trailing edge of the body being considered, with a corresponding sink at infinity or at least some considerable distance downstream. Whereas the images of the sources produce little induced velocity at the body, the sink images result in a uniform flow over the whole field.

Using this concept, and the equation $D = \rho Q U$ (D = drag and Q = source strength), the approximate relation for a two dimensional wing wake is:

(5) $$\epsilon_c = \frac{C_{D_p} C}{4H\beta^3}$$

The wing chord is C and C_{D_p} is the wing parasite drag.

The three-dimensional correction is exactly analagous to (5) above, namely:

$$\epsilon_c = \frac{C_{D_p} S}{4(BH)\beta^3} \tag{6}$$

S is the model wing area and C_{D_p} is the model parasite drag coefficient based upon S.

The final wake blocking effects to be considered were those of the strut guards. The front ones are generally in the vertical transverse plane containing the wing, allowing the use of an equation exactly similar to (6), namely:

$$\epsilon_c = \frac{(C_{D_p} S)_{SG}}{4(BH)\beta^3} \tag{7}$$

where $C_{D_p} S$ now refers to the guards.

The rear strut guard case differs slightly in that the source at its trailing edge produces a negative velocity increment at the wing. However, this effect was found to be small and (7) was recommended to have sufficient accuracy.

Knowing the values of ϵ_c for each flow component at a given M, these may be summed to give $(\Sigma \epsilon_c)_1$, and a first approximation of the corrected Mach number, M_{c_1}, calculated by the relation:

$$M_{c_1} = M\left[1 + (\Sigma \epsilon_c)_1 \left(1 + \frac{\gamma-1}{2} M^2\right)\right] \tag{8}$$

The factor $\frac{\gamma-1}{2} M^2$ approximately allows for the change in the speed of sound, a, as the speed increases from M to M_{c_1}. When M_{c_1} is de-

termined, it is possible to recalculate each ϵ_c based upon M_{av}, which is a mean between M and M_{c_1}. This results in the final values, $\Sigma\epsilon_c$ and M_c according to the equation:

$$M_c = M\left[1 + \Sigma\epsilon_c\left(1 + \frac{\gamma-1}{2}M_{AV}^2\right)\right] \tag{9}$$

M_{av} has replaced M in the correction term for a to give improved accuracy.

In addition, to allow for the change in density in proceeding from M to M_c, all force coefficients must be corrected according to the formula:

$$C_c = C\left[1 - \Sigma\epsilon_c(2 - M^2)\right] \tag{10}$$

where $C = C_L, C_D, \text{ or } C_M$.

C. Application of Thom's Method

In general, six separate corrections were applied to the results of a conventional model test. These included the solid blocking of the three-dimensional wing (Equation 2), of the fuselage (Equation 3, streamlined solid), and of the front strut guards on the model (Equation 4), as well as the wake blocking of the model itself (Equation 6), of the front strut guards on the model (Equation 7), and of the rear guard on the model (also Equation 7). The solid blocking corrections may be si ply reduced to the form $\epsilon_c = \frac{CONST.}{\beta^n}$. However, for wake blocking, the general form is $\epsilon_c = \frac{CONST. \cdot C_{D_p}}{\beta^n}$ where $C_{D_p} = C_{D_p}(M)$, since the values of C_{D_p} used were taken at the given Mach number, M.

Perhaps the best method of illustrating the use of Thom's blocking corrections is a complete sample calculation for one model. This example is shown in Appendix I for the C-69 test in the NACA Ames Aeronautical Laboratory 16 Foot circular high speed wind tunnel. Referring to Appendix I, it is seen that corrections A and B for the solid blocking of wing and fuselage respectively were easily calculated from the model dimensions. Since the wing chord (c) and the thickness (t) are not constant, mean geometrical values of each were used. For this circular tunnel, BH of equations (2) and (3) was replaced by A, the tunnel area.

As previously mentioned, the calculation of the front strut guards solid blocking required the evaluation of a constant. Thom gives the relation

$$(11) \qquad \Delta u_{A_1} = \frac{\Sigma q g}{4\pi}\left(\frac{1}{f^2+g^2}\right)\left\{\frac{\left(\frac{H}{2}+h\right)}{\sqrt{f^2+g^2+\left(\frac{H}{2}+h\right)^2}} - \frac{\left(\frac{H}{2}-h\right)}{\sqrt{f^2+g^2+\left(\frac{H}{2}-h\right)^2}}\right\}$$

(Equation 23 of Thom's paper)

$\frac{H}{2}$ = distance from tunnel center line to bottom of front strut guards.

h = height of strut guards

f = lateral distance of strut guards from the point A where the velocity increment is being calculated. A is in the vertical plane passing through the center of the guards and usually also the center of the wing.

g = longitudinal distance from center of guard or strut to line source distribution.

q = line source strength per unit length.

Although Thom does not consider it, there is also a small solid blocking correction for the wing struts themselves, which extend from the top of the guards to the wing surface. Integrating over this distance

and neglecting the images, the result is:

$$(12) \qquad \Delta u_{A_2} = \frac{\Sigma q q}{4\pi}\left(\frac{1}{f^2+g^2}\right)\left\{\frac{\left(\frac{H}{2}-h\right)}{\sqrt{f^2+g^2+\left(\frac{H}{2}-h\right)^2}}\right\}$$

Figure 9 of Thom's report, which was reproduced for the circular tunnel application in Figure 2, shows the above mentioned dimensions. The point A was taken at the center of the tunnel, since this point has previously been shown to give a mean value over the model. Then f is half the distance between the two front strut guards. Plots of $\frac{g}{\pi t}$ and $\frac{q}{c}$ as a function of thickness ratio, $\frac{t}{c}$, are given in Figure 4 of Thom's paper which has been reproduced in Figure 3. Shape B, which is essentially a Rankine oval, was used. Since $g^2 = c^2\left(\frac{g}{c}\right)^2$ and $qq = \pi tc\left(\frac{g}{\pi t}\right)\left(\frac{q}{c}\right)$, equations (11) and (12) were combined to the form:

$$(13) \qquad \Delta u_A = \Delta u_{A_1} + \Delta u_{A_2} = \text{CONST.} \times u\left[(tc)_{\text{GUARD}} + (tc)_{\text{STRUT}}\right]$$

(for 1 strut and guard)

Inasmuch as $\frac{\Delta u_A}{u} = \epsilon$ and $\epsilon_c = \frac{\epsilon}{\beta^n}$ and the chord and thickness of the guard and struts were known, the front strut and guard solid blocking was fully determined. It is to be noted, however, that this correction involves the assumption of a flat tunnel floor separating the strut guards and their mirror images. This should not incorporate a very large error because the primary effect on the model is from the guards themselves and this effect is not a function of tunnel shape. Although the solid blocking of the rear strut and guard produces a small negative velocity increment at the wing, its effect was counterbalanced by also neglecting the solid blocking of the front guard stiffening struts and wires. The only exceptions in which the effect of the rear

guards at A were considered were the B-29 test , in which the rear guard was considerably larger than the front ones, and the XP-51 in which there were no front guard stiffening struts and the rear guard had a large chord.

Proceeding to the wake blocking of the model (Correction D), the first step was the reduction of the drag data to remove the induced drag. Table I, Appendix I, gives values of C_{D_P} for the range of tunnel Mach numbers and lift coefficients considered. Table II gives the values of the model wake blocking, $\epsilon_{c_D}/\beta^3 = CONST. C_{D_P}$ for the same range of M and C_L.

Equation (7) was used to determine ϵ_{c_E} and ϵ_{c_F}, the wake blocking correction factors for the front and rear strut guards respectively. The circular tunnel area, A, replaced the factor BH just as in the other four correction terms. Incidentally, although the circular area of the Ames 16 Foot Tunnel is 201 square feet, 195 was used to account for the boundary layer growth and the flat side walls which are used to facilitate two dimensional testing. The values of C_{D_P} used were derived from Figure 1, Appendix I, which is a non-dimensional plot of parasite drag ratio against Mach Number ratio. The two curves, a and b, were calculated from the wing alone data of the XB-42 and XSB2D-1 models respectively and were not corrected for blocking. Curve a, which was used for the C-69, corresponds to models of moderately large blocking, and b is for tests having smaller blocking. For the C-69 front guards having a thickness ratio ($\frac{t}{c}$) of .133, $C_{D_{P_{INC}}}$ was taken as .0065 and M_{cr} as .71. The numerical values for the correc-

tion term $\epsilon_{c_E} \beta^3$ for the front guards were calculated in Table III (Appendix I). S is the "wing" area of both guards and the smaller bracing struts. The rear guard was treated in the same manner, using $C_{D_{P_{INC}}} = .0070$ and $M_{cr} = .69$ for a thickness ratio of .159. The calculation of $\epsilon_{c_F} \beta^3$ is given in Table IV.

Next, ϵ_{c_A}, ϵ_{c_C}, ϵ_{c_D}, ϵ_{c_E}, AND ϵ_{c_F}, all of which include the factor β^3 were summed and numerical values obtained for the complete range of M and C_L (Table V). This table also includes a column for ϵ_{c_B} which has the factor β^4 and is not a function of C_L. The factors $\frac{1}{\beta^3}$ and $\frac{1}{\beta^4}$ were read from Figure 1. Addition of the latter column of ϵ_{c_B} to the other values of ϵ_c at the corresponding M's gave $\Sigma \epsilon_c$, in Table VI. Application of Equation (8) resulted in the values of M_{c_1} listed in Table VII. Then the operations of Tables V and VI were repeated in Tables VIII and IX respectively, using $M_{AV} = \frac{M + M_{c_1}}{2}$ in place of M in getting $\frac{1}{\beta^3}$ and $\frac{1}{\beta^4}$. Table IX now contained a tabulation of $\Sigma \epsilon_c$ from which M_c was calculated in Table X according to Equation (9). For convenience in correcting the critical Mach numbers for blocking effect, $(M_c - M)$ was calculated in Table XI. Actually, this table was superfluous in the case of the C-69 in which $(M_{cr})_c$ was obtained from airfoil section data, and $(M_c - M)$ was plotted in Figure 2, Appendix I for the B-42 instead. Next the drag coefficients were corrected according to equation (10) and tabulated in Table XII. It is to be noted that C_L also decreases as M increases. Finally, the corrected drag ratio, $\left(\frac{C_D}{C_{D_{INC}}}\right)_c$, where $\left(C_{D_{INC}}\right)_c$ was taken at the lowest available Mach number, M, (.3 for the C-69) was calculated in Table XIII.

The dimensions of the struts and guards used in the various tests in the Ames 16 Foot Tunnel are given in Table XV.

The above method leading to M_c and $\left(\frac{C_D}{C_{DINC}}\right)_c$ was repeated with only minor individual modifications for the P-38, P-58, and B-29 models as well as the C-69. It is to be noted that Thom's corrections are based upon a tunnel empty calibration, which was the case for the above 4 tests. However, the P-51B, XP-51, B-42, P-47, and XSB2D-1 tests were calibrated with the struts and strut guards in place. Therefore, corrections C, E, and F for the solid and wake blocking of the struts and guards were omitted in these models.

D. Discussion

It has been seen throughout the preceding pages, that the one large weakness was the application of Thom's rectangular tunnel results to tests run in a circular wind tunnel. Therefore, certain cases were investigated with the view of developing analagous circular tunnel expressions. However, considerable mathematical difficulties arose because the system of a point source inside a circular cylinder and its image will not satisfy the condition of no flow across the boundary unless a sink of appropriate strength is placed in the center of the tunnel section. The presence of this sink obviously alters the flow pattern inside the tunnel so that it no longer corresponds to reality. In addition, a mathematical singularity is encountered in that a source at the center of the tunnel has its image at infinity. Therefore, the simple methods of images which work for the rectangular tunnel are not practicable for the circular tunnel and more complicated

and elegant methods must be used. Further investigation of this problem with a view toward a solution analagous to Thom's is highly desirable; in fact it might be said that it is urgently necessary.

As a check, however, correction B for a body of revolution (fuselage) was also calculated by the method of Lock for a circular tunnel in R and M 1451 (Reference 5). In all but two cases, exactly the same result was obtained. As a further check, the body solid blocking correction (B) was also calculated by the more exact method of Lamb[7] for the P-51B fuselage. Thom's approximation gave $\epsilon_{c_B} = \frac{.0028}{\beta^4}$ for this model, which was within ten per cent of the result obtained using Lamb's method and the Prandtl Glauert Approximation at M = .8. These facts indicate that for this particular shape of rectangular tunnel $\left(\frac{B}{H} = \frac{3}{2}\right)$, corrections based upon a body representation by point sources and sinks differ little from circular tunnels. A further indication of this may be seen from the fact that the low speed wind tunnel wall correction factors are almost identical for small wings in a 3 x 2 rectangular and a circular tunnel. (See reference 6). Therefore, the body correction and all three wake blocking corrections, which are also based on point sources and sinks, may be considered as fairly reliable. Also, as previously stated, the solid blocking effect of the strut guards on the model (correction C) is to a first approximation independent of tunnel shape. This leaves only the three dimensional wing blocking (correction A) which is of dubious accuracy. Fortunately, the magnitude of this factor is small compared with the fuselage correction.

It is also to be noted that the correction factors used are based on the Prandtl-Glauert approximation and are strictly applicable only in a flow which is subsonic in the entire region. This criterion is, of course, no longer satisfied when the lowest critical Mach number of the model and its support systems is reached and shock waves are possible. Because of the extreme complexity of mixed (sub and supersonic) flow problems and the consequent lack of information, the factors herein outlined were used through the entire range of Mach number, M. It has been suggested that the error is not too considerable until the shock waves strike and are reflected from the tunnel wall.

The model solid blocking factors were derived under the assumption of zero angle of attack. These corrections (A and B) were used directly without considering any variation of model angle of attack, α, from zero. However, this error is expected to be quite small since the range of C_L from 0 to .5 will straddle a zero mean α for most models. In other words, the range of angle of attacks for these values of C_L was usually from -2.5° to $+ 2.5^\circ$.

Appendix I shows the large magnitude of the overall blocking correction. The question then arises as to possible means of reducing this effect to a practicable minimum. The obvious solution is, for a given tunnel, to test the smallest size model consistent with Reynolds number considerations and support it by the smallest struts consistent with structural limitations. The struts should be made of high speed, laminar flow sections of minimum thickness ratio to reduce their drag and increase their critical Mach number. Since the "choking

speed" or maximum attainable value of M regardless of power input is largely a function of model size, a reduction in the latter would also serve to increase tunnel performance. An adaptation of supersonic flow technique of supporting the model from the rear by a single strut might also be used to reduce the blocking effect.

Because of the tremendous mathematical complications involved in mixed flow problems, it seems that empirical methods must be used at the higher Mach numbers (.75 to 1.00). In view of the large amount of data of dubious value now in existence and the urgency of the problem, a comprehensive experimental program should be initiated. This program might include three dimensional tests using different sizes of struts and strut guards to enable extrapolation to zero size. Having independently obtained the strut effect, the same procedure may be used for different scales of the same model. A separate investigation of scale effect preferably by the use of variable density would also be necessary using this type of a proach. The same process could also be carried out two-dimensionally with the simplification of the absence of struts. In addition, complete velocity surveys of the flow fields would be highly informative.

CLASSIFICATION cancelled

IV Calculation of Wing Critical Mach Numbers

One of the two basic parameters used in plotting all results was the Mach number ratio, $\left(\frac{M}{M_{cr}}\right)$, where M_{cr} is, as usual, defined as that value of M which first produces sonic velocity at the wing section under consideration. It is expected that the critical Mach number varies along the wing span and therefore M_{cr} for any wing of a given airplane at a given lift coefficient was taken as a mean value. Whenever possible, this mean was determined by

$$M_{cr} = \frac{1}{\frac{S}{2}} \int_0^{\frac{b}{2}} m_{cr} c \, dy \tag{14}$$

where:

m_{cr} = local critical Mach number

S = wing area

c = local wing chord

b = wing span

y = variable of span

Such a process simply involved a plot of $m_{cr}c$ along the semispan, integration, and division by half the wing area. In some cases, tunnel or flight wing pressure distributions were unavailable and only the root and tip airfoil sections were known. Under such conditions, M_{cr} was also determined by the averaging process of equation (14) assuming a linear variation between the root and tip values of $m_{cr}c$. The principal problem, however, was the calculation of m_{cr} both in the wind tunnel and in the free stream. The wind tunnel case will be discussed first.

CLASSIFICATION cancelled

At each Mach number, there exists a unique critical value of wing pressure coefficient, P_{cr}, which corresponds to sonic velocity. P is defined as:

(15) $$P = \frac{p - p_\infty}{\frac{1}{2} \rho_\infty U_\infty^2}$$

where: p = local static pressure

p_∞ = model reference static pressure

ρ_∞ = model reference density

U_∞ = model reference velocity

In flight, p_∞ and ρ_∞ are the ambient pressure and density respectively and U_∞ is the flight velocity.

Hence,

$$P = \frac{2 p_\infty}{\rho_\infty U_\infty^2}\left(\frac{p}{p_\infty} - 1\right) = \frac{2}{\gamma}\frac{1}{M_\infty^2}\left(\frac{p}{p_0}\frac{p_0}{p_\infty} - 1\right)$$

$$a_\infty^2 = \frac{\gamma p_\infty}{\rho_\infty}, \qquad M_\infty^2 = \frac{U_\infty^2}{a_\infty^2}$$

for isentropic flow from rest (p_0 = stagnation pressure):

$$\frac{p}{p_0} = \frac{1}{\left(1 + \frac{\gamma-1}{2} M^2\right)^{\frac{\gamma}{\gamma-1}}}$$

and

$$\frac{p_0}{p_\infty} = \left(1 + \frac{\gamma-1}{2} M_\infty^2\right)^{\frac{\gamma}{\gamma-1}}$$

then,

$$P = \frac{2}{\gamma}\frac{1}{M_\infty^2}\left[\left(\frac{1 + \frac{\gamma-1}{2} M_\infty^2}{1 + \frac{\gamma-1}{2} M^2}\right)^{\frac{\gamma}{\gamma-1}} - 1\right]$$

finally, since M = 1 for $P = P_{cr}$,

(16) $$P_{cr} = \frac{2}{\gamma M_\infty^2}\left[\left(\frac{1+\frac{\gamma-1}{2}M_\infty^2}{1+\frac{\gamma-1}{2}}\right)^{\frac{\gamma}{\gamma-1}} - 1\right]$$

For simplicity and consistency with wind tunnel notation, the subscript ∞ was dropped, giving:

(17) $$P_{cr} = \frac{2}{\gamma M^2}\left[\left(\frac{1+\frac{\gamma-1}{2}M^2}{1+\frac{\gamma-1}{2}}\right)^{\frac{\gamma}{\gamma-1}} - 1\right]$$

Equation (17) is plotted on figure 1 of Appendix II.

Knowing the pressure distribution at various values of Mach number, it is customary to plot P_{MAX} against M for constant values of angle of attack in order to obtain m_{cr}. The intersection of the curve of P_{MAX} and P_{cr} gives the desired m_{cr}. For those tests in which wing pressure distributions were available, a process of interpolation was necessary to obtain a curve of P_{MAX} at constant α (local angle of attack) and yet have m_{cr} correspond to a given lift coefficient of the model. Since m_{cr} was known approximately, the angles of attack at the desired C_L were read at two values of M, m_a and m_b, which straddle m_{cr}. It was then possible to estimate α_{cr} very closely. Using this value of α_{cr}, an interpolation of the pressure distributions yielded values of $(P_{MAX})_a$ and $(P_{MAX})_b$ corresponding to α_{cr} and m_a and m_b respectively. This is shown graphically in Figure 1 of Appendix II. The curve joining a and b is for a constant angle of attack, α_{cr}, and the intersection with the P_{cr} curve gives m_{cr} at the desired lift coefficient. This process was repeated for values of C_L of 0, .1, .2, .3, .4, and .5

CONFIDENTIAL
CLASSIFICATION cancelled

and at each wing station where pressure readings were taken. Now knowing the variation of m_{cr} with span at each lift coefficient, the corresponding values of mean critical Mach number, M_{cr}, were calculated by the method previously outlined by equation (14). Figures 2 and 3 of Appendix II show a sample determination of m_{cr} at the wing stations and of M_{cr} for the B-42 at $C_L = 0$.

In those tests in which wing pressure distributions were made, it was necessary to apply the same blocking correction as for the drag data because each pressure distribution was for a tunnel Mach number, M. The correction might have been inserted immediately at the beginning of the critical Mach number calculations, but it was considered simpler to determine the uncorrected M_{cr} and from this to calculate the corresponding free stream value, $(M_{cr})_c$. After the blocking corrections were determined for each model test, a plot of $(M_c - M)$ against M was made. Figure 2 in the sample blocking effect calculations of Appendix I is an example of these curves for each value of C_L in the 0 to .5 range considered. Thus it was a simple matter to insert M_{cr} on the M scale and pick off the correction at the corresponding value of C_L. Knowing the correction, $(M_c - M)$, the free stream (corrected) critical Mach number is $(M_{cr})_c = M_{cr} + (M_c - M)_{M = M_{cr}}$.

It may be noted that an increase in the Mach number from the wind tunnel to the free stream is also accompanied by a corresponding decrease in pressure coefficient, P, which is of correct magnitude to return the final point (flight condition) to the curve of P_{cr}. The relation for the free stream pressure coefficient in terms of the

CONFIDENTIAL
CLASSIFICATION cancelled

CLASSIFICATION cancelled

tunnel value and the corresponding Mach numbers which is the basis for the preceding statement may be easily derived. The tunnel pressure coefficient is defined as:

$$P_m = \frac{p - p_m}{\frac{1}{2}\rho_m U_m^2} \tag{18}$$

where p_m is the measured tunnel reference static pressure in the plane of the model, but far from it. The flight coefficient is defined as:

$$P_{FS} = \frac{p - p_{FS}}{\frac{1}{2}\rho_{FS} U_{FS}^2} \tag{19}$$

where p_{FS} is the ambient static pressure. In both definitions, p is the pressure at any point on the airplane or model; it is a physically measured quantity and invariant between the wind tunnel and flight. Then,

$$p = P_{FS} \cdot \tfrac{1}{2}\rho_{FS} U_{FS}^2 + p_{FS} = P_m \cdot \tfrac{1}{2}\rho_m U_m^2 + p_m$$

dividing by p_{FS},

$$\frac{P_{FS} \cdot \frac{1}{2}\rho_{FS} U_{FS}^2}{p_{FS}} + 1 = \frac{P_m \cdot \frac{1}{2}\rho_m U_m^2}{p_{FS}} + \frac{p_m}{p_{FS}}$$

$$\frac{P_{FS} \cdot \frac{1}{2}\rho_{FS} U_{FS}^2}{p_{FS}} \cdot \frac{\gamma}{\gamma} + 1 = \frac{p_m}{p_{FS}} \cdot \left[1 + \frac{P_m \cdot \frac{1}{2}\rho_m U_m^2}{p_m} \cdot \frac{\gamma}{\gamma} \right]$$

since $\frac{\gamma p}{\rho} = a^2$ AND $\frac{U^2}{a^2} = M^2$

CLASSIFICATION cancelled

$$(20) \qquad P_{FS}\frac{\gamma}{2}M_{FS}^2 + 1 = \frac{\rho_m}{\rho_{FS}}\left[1 + P_m \cdot \frac{\gamma}{2}M_m^2\right]$$

For flow from rest,

$$\rho_m = \rho_0\left(1 + \frac{\gamma-1}{2}M_m^2\right)^{-\frac{\gamma}{\gamma-1}}$$

and

$$\rho_{FS} = \rho_0\left(1 + \frac{\gamma-1}{2}M_{FS}^2\right)^{-\frac{\gamma}{\gamma-1}}$$

Then,

$$\frac{\rho_m}{\rho_{FS}} = \left(\frac{1 + \frac{\gamma-1}{2}M_{FS}^2}{1 + \frac{\gamma-1}{2}M_m^2}\right)^{\frac{\gamma}{\gamma-1}}$$

Substituting into (20),

$$P_{FS}\frac{\gamma}{2}M_{FS}^2 + 1 = \left(\frac{1 + \frac{\gamma-1}{2}M_{FS}^2}{1 + \frac{\gamma-1}{2}M_m^2}\right)^{\frac{\gamma}{\gamma-1}}\left(1 + P_m \cdot \frac{\gamma}{2}M_m^2\right)$$

Solving for P_{FS}:

$$P_{FS} = \left[\frac{1 + \frac{\gamma-1}{2}M_{FS}^2}{1 + \frac{\gamma-1}{2}M_m^2}\right]^{\frac{\gamma}{\gamma-1}}\left[\frac{2}{\gamma M_{FS}^2} + P_m\left(\frac{M_m}{M_{FS}}\right)^2\right] - \frac{2}{\gamma M_{FS}^2}$$

Removing the subscript m for simplicity and consistency with previous wind tunnel notation, and replacing M_{FS} and P_{FS} by the corrected Mach number and pressure coefficient, M_c and P_c, which are equivalent, the final result is:

$$(21) \qquad P_c = \left[\frac{1 + \frac{\gamma-1}{2}M_c^2}{1 + \frac{\gamma-1}{2}M^2}\right]^{\frac{\gamma}{\gamma-1}}\left[\frac{2}{\gamma M_c^2} + P\left(\frac{M}{M_c}\right)^2\right] - \frac{2}{\gamma M_c^2}$$

For example, in the B-42 at $C_L = 0$, as M_{cr} was corrected from .677 to .685, the pressure coefficient was correspondingly increased from -.857 to -.844 according to equation (21). Thus the uncorrected P_{cr} and M_{cr} were corrected for blocking effect and the resulting point remained on the sonic curve (Eq. 17).

The problem was considerably simpler in those tests which required the use of airfoil section data in the absence of wing pressure distributions, although the resulting values of M_{cr} are not expected to be as reliable. All the experimental air oil data were obtained from two-dimensional tunnel tests and the only correction which had to be applied was the one for blocking effect. Usually, the airfoil sections were known only at the wing root and tip. This yielded two values for $m_{cr}c$ from which, as previously mentioned, M_{cr} was determined by equation (14) assuming a linear variation of $m_{cr}c$ along the span. Actually, a corrected curve of normal force coefficient (C_N) or C_L vs. $(m_{cr})_c$ was plotted with the uncorrected one and the former was used to get $(m_{cr})_c$ and hence $(M_{cr})_c$ directly. The two dimensional solid blocking factor of equation (3) and the coefficient correction of equation (10) were applied to the airfoil data. The wake blocking correction for these two-dimensional sections was negligible. Since each point on such a curve of C_N or C_L vs. m_{cr} is for a definite angle of attack, α, of the section, it was simpler to relate the same values of α to those of the model test. Assuming that the model angles are measured from the fuselage reference line, α at any point along the span was known in terms of the model angle of attack from given geometrical

characteristics. The test results gave the model α at all lift coefficients and Mach numbers. Hence, the angles of attack at the wing root and tip sections were known for any value of model C_L and Mach number, enabling direct use of the section plot to select $(m_{cr})_c$. An example of these plots of airfoil critical Mach number is seen in Figure 4 (Appendix II) for the NACA 23015 section.[16]

Some flight tests made to determine drag characteristics also included wing pressure distributions at one or more stations along the span. The process for calculating the critical Mach numbers is the same as in the wind tunnel except that, of course, no correction for blocking effect is necessary. At each wing station, the maximum pressure coefficient was plotted against Mach number and the intersection with the P_{cr} curve of equation (17) gave $(m_{cr})_c$ directly. The averaging process of equation (14) then yielded $(M_{cr})_c$. This latter value was for a lift coefficient at or very close to zero for all flight dive tests. No level flight high speed data were available. In at least one instance, however, flight experimental data for the calculation of the wing critical Mach number was not taken and it was necessary to use the value of $(M_{cr})_c$ at $C_L = 0$ for the same model.

Table II contains a tabulation of all calculated values of $(M_{cr})_c$ in the desired range of lift coefficients for all tests, wind tunnel and flight, used in this report. The method by which the critical Mach numbers were obtained is also indicated in each case.

The superiority of high speed, low drag airfoil sections, both in their higher critical Mach numbers at zero lift coefficient,

CLASSIFICATION cancelled

and in their considerably less rapid decrease in $(M_{cr})_c$ as C_L increases is shown in Table II.

The critical Mach numbers for the P-47 at the higher lift coefficients are considered very doubtful even though they are from experimental section data. Since the airfoil does not correspond to an N.A.C.A. section, it was not possible to check the values and they had to be used as given in the table.

Finally, with the values of $(M_{cr})_c$ determined, the Mach Number ratio, $\left(\frac{M}{M_{cr}}\right)$, was calculated. An example of this was done for the C-69 and included in Appendix I as Table XIV.

CLASSIFICATION cancelled

CONFIDENTIAL
CLASSIFICATION cancelled

Table II - A Tabulation of $(M_{cr})_c$

Test	Airfoil		$(M_{cr})_c$ Free Stream or Corrected						Method of Calculation	Remarks	Reference
	Root	Tip	$C_L = 0$	$C_L = .1$	$C_L = .2$	$C_L = .3$	$C_L = .4$	$C_L = .5$			
			Wind Tunnel Tests								
B-29	Boeing 117 $\frac{t}{c} = .22$	Boeing 117 $\frac{t}{c} = .09$	.611	.604	.597	.590	.582	.572	A		14
B-42	G-17	G-17	.685	.676	.667	.659	.651	.642	A	Douglas G-17 High Speed Section, $\frac{t}{c} = .17$	19
C-69	23018	4412	.632	.625	.607	.583	.561	.539	B		15 and 16
P-38	23016	4412	.641	.626	.600	.575	.549	.525	B		15 and 16
P-47	S-3 $\frac{t}{c} = .16$	S-3 $\frac{t}{c} = .09$	.691	.664	.627	.588	.544	.494	B	Republic S-3 Airfoil Section	10
XP-51	NAA $\frac{t}{c} = .1607$	NAA $\frac{t}{c} = .1144$	.705	.694	.682	.669	.658	.643	A	North American High Speed Section	23
P-51B	NAA $\frac{t}{c} = .1607$	NAA $\frac{t}{c} = .1144$	.698	.685	.677	.666	.653	.635	A	North American High Speed Section	24 and 25
P-58	23016	4412	.644	.627	.603	.583	.558	.537	B	Constant 23016 Section to Station 220	15 and 16
P-58	66,2-116	66,2-216	.698	.694	.685	.670	.655	.635	A and B	B is Theoretical Airfoil Data of Ref. 17 in this case	17 and 26
XSB2D-1	ES XX,25-218	65,2-2515	.674	.666	.659	.653	.646	.635	A	Root has Douglas El Segundo High Speed Section; $\frac{t}{c} = .18$	27

CONFIDENTIAL
CLASSIFICATION cancelled

CLASSIFICATION CONFIDENTIAL Cancelled

Table II (Continued)

Test	Airfoil		$(M_{cr})_c$ Free Stream or Corrected						Method of Calculation	Remarks	Reference
	Root	Tip	$C_L = 0$	$C_L = .1$	$C_L = .2$	$C_L = .3$	$C_L = .4$	$C_L = .5$			
						Flight Tests					
XF2A-2	23014	23014	.640	-	-	-	-	-	C		13
P-47	S-3 $\frac{t}{c} = .16$	S-3 $\frac{t}{c} = .09$	.691	-	-	-	-	-	B		10

A - Tunnel Wing Pressure Distributions

B - Airfoil Section Data

C - Flight Wing Pressure Distributions

All Airfoils are NACA Sections Unless Otherwise Stated

CLASSIFICATION CONFIDENTIAL Cancelled

CONFIDENTIAL
CLASSIFICATION cancelled

V Results

After all of the corrections were applied to the wind tunnel results, several methods of correlation were tried. It was necessary to find some way to non-dimensionalize the data in a convenient manner for it to be used to design new aircraft. The best way appears to be a graph of $\left(\frac{C_D}{C_{D_{INC}}}\right)$ versus $\left(\frac{M}{M_{cr}}\right)$ where the $C_{D_{INC.}}$ is the low speed drag and the M_{cr} is the average value of the local critical Mach numbers over the wing. The use of $\left(\frac{M}{M_{cr}}\right)$ as a primary parameter in this empirical attempt to find a universal drag function is largely dependent upon the wing having a lower critical Mach number than any other part of the airplane. When this is not the case, discrepancies will occur which cannot be accounted for with the present method. However, basing the increase in drag on the critical Mach number of the wing appears to give a reasonable approximation to the answer because the drag of the wing is the largest part of the total drag of the airplane.

Figures 4 - 13 show $\left(\frac{C_D}{C_{D_{INC}}}\right)_c$ versus $\left(\frac{M}{M_{cr}}\right)_c$ for each of the airplanes considered. There are five models having conventional airfoils and five with low drag sections. A separate curve is drawn for each lift coefficient from 0 to .5 by tenths. The variations are generally regular, moving to the right as the lift coefficient increases. It might be pointed out that $(M_{cr})_c$ corresponds to the lift coefficient which is being considered, and since $(M_{cr})_c$ decreases with increasing C_L the curves progressively move to the right. However, for one airplane, the B-29, there is only one curve for all

CONFIDENTIAL
CLASSIFICATION cancelled

lift coefficients. Since the critical Mach numbers were determined from pressure distributions made directly on the B-29 wing at several stations, they are reliable, and therefore no reason can be given for this peculiarity. Figure 7 for the P-47 is not in agreement with the drag ratio curves of other airplanes (Figures 4-8) at lift coefficients over .2. The critical Mach numbers were determined from tests of an airfoil corresponding to the P-47 wing at the aileron mid-point station and were corrected for blocking effect and thickness variation. The results seem to be rather odd in that the critical Mach number is quite high at zero lift but falls off extremely rapidly as the lift increases. This accounts for the low rate of increase of drag at the high lift coefficients. If the variation in critical Mach number with lift coefficient conformed to the usual type of variation, the drag curves would be more normal.

Figure 14 shows the non-dimensional drag increase for airplanes with conventional wings at zero lift. This curve has very little scatter for the five airplanes considered and provides the desired result if it agrees with the flight tests. Figures 15 - 19 are the same type curves for lift coefficients of .1, .2, .3, .4 and .5. In the two latter curves it was necessary to limit the maximum $\left(\frac{M}{M_{cr}}\right)_c$ to 1.3 because of excessive scatter at higher values.

Figures 20-25 show the drag increase for five airplane models with low drag airfoil sections. The scatter which appears in these curves may be accounted for in several ways: 1) Tare drags are measured without taking the interference between struts and model into consideration. 2) Since the airfoil sections are not the same on the

various models, the pressure distributions also vary, and therefore the shock waves build up in different manners. 3) Each airplane differs in other parts as well as wing, and these parts cause drag increases which occur at varying Mach numbers. Although considerable scatter does exist in these curves, they are sufficiently well defined to be useful.

It was necessary to draw separate correlation curves for airplanes having conventional wings and those having low drag wings for the following reasons: 1) The turbulence increases from a low level at small Mach numbers to a higher level at the larger Mach numbers. A low drag wing, which has a laminar flow region at low turbulence, tends to lose its low drag characteristics at high turbulence. Thus, a laminar flow wing has a greater percentage increase in drag than a conventional wing at the same Mach number because of this phenomenon. 2) The increase in drag is based on the critical Mach number of the wing and does not consider other items of the model. Since the critical Mach number of low drag airfoils is in general higher than that of conventional sections, the actual Mach number at the same $\left(\frac{M}{M_{cr}}\right)_c$ is greater for the low drag airfoil case. Then the other components such as cowling, ducts, and canopies are operating at higher ratios of Mach number to their indidivual critical Mach numbers and therefore at higher drag. 3) When M is supercritical, the shock wave of the low drag airfoil is stronger than that of the conventional airfoil at the same $\left(\frac{M}{M_{cr}}\right)_c$.

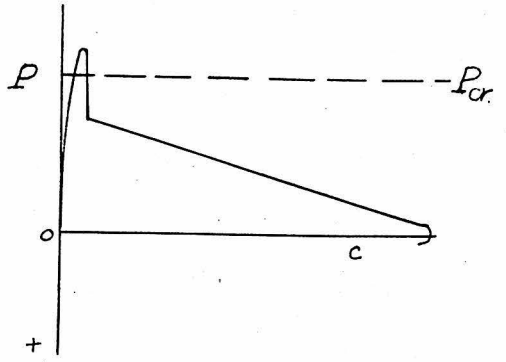

Conventional Wing

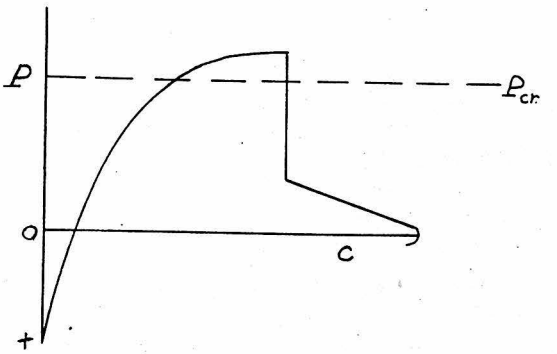

Low Drag Wing

This is true because the shock wave on a low drag section occurs farther downstream and a greater pressure recovery is necessary (see sketch).

The only available flight tests which were considered reasonable were those performed on the Brewster XF2A-2[13] and the P-47[30]. The results of these tests were non-dimensionalized and plotted in Figure 26 along with a dashed wind tunnel curve for conventional airfoils at zero lift. The agreement is quite good, but it is obvious that more data are necessary to provide a satisfactory check. High speed flight test drag results are not available at present on airplanes using low drag airfoil sections. However, dive tests on the XP-51 are now in progress.

Figures 27 and 28 are the final design curves to be used in predicting the drag of an airplane at any Mach number. The incompressible drag coefficient and the critical Mach number of the wing must be estimated from the design of the airplane. Then, calculating the C_L corresponding to the Mach number at which the drag is to be calculated, Figure 27 or 28 is entered with $\left(\frac{M}{M_{cr}}\right)_c$ and $\left(\frac{C_D}{C_{D_{MC}}}\right)_c$ is read at the appropriate lift coefficient.

CLASSIFICATION cancelled

VI Conclusions

The objective of this investigation was accomplished in that empirical relations giving the increase in drag with Mach number were obtained. Although these curves are not considered completely accurate they may be regarded as the best results available at present. In the future when more reliable tests have been made, it will be possible to improve these results. It is not reasonable to expect that an accurate curve of drag increase of the total airplane with Mach number based only on the critical Mach number of the wing can be obtained, because of the influence of the other components of the airplane such as the engine cowlings, scoop entrances, pilot canopies, turrets, wing-fuselage fillets, and wing nacelle fillets. Although one could probably derive a universal curve or family of curves for wings or for any other one part, it is not logical to assume that there is a universal function for a combination of wing, fuselage, nacelles, etc. To get a truly reliable answer, it is expected that it will be necessary to base the increase in drag of each part of the airplane on its individual critical Mach number and possibly other parameters of that part should they prove important. Then the drag of the separate parts could be summed at each Mach number to arrive at a total drag estimate of the entire airplane.

Another method that might be used to account for the other parts of the airplane is to define a "cleanness" factor which would be dependent upon the ratio of the critical Mach numbers of each of the other parts of the airplane to that of the wing. The ratio for each part would be weighted according to its importance in relation

CLASSIFICATION cancelled

to the other parts. Thus, a universal drag function might be obtained at each constant value of this cleanness factor. Another consideration which might measurably affect the results is a considerable variation of maximum difference between M_{cr} and m_{cr} at constant C_L of the wings of the different airplane and model tests considered. This effect was rather marked at the crank of the gull-winged XSB2D-1 where m_{cr} fell considerably below M_{cr}. Such a condition causes a premature formation of shock waves and an earlier rise of the model total drag coefficient. Fortunately, the maximum variation of m_{cr} from M_{cr} was quite uniform for the continuous wings of the other tests.

If a conventional airplane is being considered, the general method given in this report may be used with reasonable accuracy, but for a flying wing or an airplane of radical design, a more complicated method such as was suggested above would be necessary.

More flight tests at high speed are advisable to provide a check for the wind tunnel results used herein. Judging from the flight test data inspected, it is felt that considerable development work on flight test instrumentation is necessary.

Further wind tunnel testing may be considered of definite value, providing care is exercised in the selection of model and support strut sizes and configuration, in the tunnel calibration, and in the analysis and correction of the resulting data. The blockings corrections used in this report may be considered a good engineering approximation pending an extension of Thom's methods to the case of a circular wind tunnel.

CLASSIFICATION cancelled

VII Recommendations

It is recommended that:

1. The final results of this analysis given in Figures 27 and 28 be used in estimating drag at high speeds.

2. Wind tunnel data be corrected for blocking effect by the methods outlined in section III.

3. Thom's method for computation of blocking corrections be extended to the case of the circular wind tunnel.

4. A comprehensive program to experimentally determine the blocking effect be initiated.

5. Flight test instrumentation suitable for terminal velocity dives be developed.

6. Some of our present fighter planes be dived to high speeds with the best available flight test instrumentation installed.

7. Special large size models or full size airplanes motivated by high powered rockets or ramjets of short duration be constructed with the sole purpose of determining high speed effects.

CLASSIFICATION cancelled

VIII References

1. A. Thom — Blockage Corrections and Choking in the R.A.E. High Speed Tunnel, British RAE Report No. Aero. 1891, November 1943.

2. S. Goldstein and A. D. Young — The Linear Perturbation Theory of Compressible Flow With Applications to Wind Tunnel Interference, British ARC 6865, Ae 2262 FM 601, July 6, 1943.

3. H. S. Tsien and L. Lees — The Glauert-Prandtl Approximation for Subsonic Flows of a Compressible Fluid, Unpublished Report at GALCIT, March, 1944.

4. C. N. H. Lock — The Interference of a Wind Tunnel on a Symmetrical Body, British ARC R. and M. 1275, 1930.

5. C. N. H. Lock and F. C. Johansen — Wind Tunnel Interference on Streamline Bodies, British ARC R. and M. 1451, 1933.

6. H. Glauert — Wind Tunnel Interference on Wings, Bodies, and Airscrews, British ARC R. and M. 1566, 1933.

7. H. Lamb — On the Effect of the Walls of an Experimental Tank on the Resistance of a Model, British ARC R. and M. 1010, January, 1926.

8. G. E. Nitzberg — The Effect of Compressibility of Two Dimensional Wall Interference for a Symmetrical Airfoil, NACA ARR 3E28, Ames Aeronautical Laboratory, May, 1943.

9. F. W. Geiger — An Approximate Constriction Correction for High Speed Closed Throat Wind Tunnel Data, Curtiss Research Laboratory Report 5A-23, March 24, 1944.

10. A. A. Luomia — Effect of Compressibility on Pressure Distribution Over an Airfoil With a Slotted Frise Aileron, NACA ACR L4G12, Langley Memorial Aeronautical Laboratory, July, 1944.

11. M. A. Heaslet — Critical Mach Numbers of Various Airfoil Sections, NACA ACR 4G18, Ames Aeronautical Laboratory, July 18, 1944.

12. T. Theodorsen and A. Regier — Experiments on Drag of Revolving Discs, Cylinders and Streamline Rods at High Speeds, NACA ACR L4F16, Langley Memorial Aeronautical Laboratory, June, 1944.

13. R. V. Rhode and H. A. Pearson — Observations of Compressibility Phenomena in Flight, NACA ACR 3D15, Langley Memorial Aeronautical Laboratory, April, 1943

14. R. H. Barnes — High Speed Aerodynamic Characteristics of the XB-29 Airplane as Determined from Tests of a .075 Scale Model, NACA ACR, Ames Aeronautical Laboratory, January 8, 1944.

15. J. Stack, W. F. Lindsey, and R. E. Littell — The Compressibility Burble and the Effect of Compressibility on Pressures and Forces Acting on an Airfoil, NACA TR 646, Langley Memorial Aeronautical Laboratory, July 6, 1938.

16. Pressure Distribution Data for an NACA 23015 Airfoil at High Speeds, NACA Preliminary Data, Langley Memorial Aeronautical Laboratory, December 16, 1942.

17. E. N. Jacobs, I. H. Abbott, and M. Davidson — Preliminary Low Drag Airfoil and Flap Data from Tests at Large Reynolds Numbers and Low Turbulence (With Supplement), NACA ACR, Langley Memorial Aeronautical Laboratory, March, 1942.

18. 16-Foot Wind Tunnel Tests of the Boeing XC-97 Airplane Model, NACA Preliminary Data, Ames Aeronautical Laboratory, April 14, 1943.

19. Wind Tunnel Tests of a .175 Scale Model of the XB-42 Airplane, NACA Preliminary Data, Ames Aeronautical Laboratory, February 12, 1944 to March 29, 1944.

20. 16-Foot Wind Tunnel Tests of C-69 Airplane Model, NACA Preliminary Data, Ames Aeronautical Laboratory, December 3, 1942.

21. 16-Foot Wind Tunnel Tests of the Lockheed P-38 Model, NACA Preliminary Data, Ames Aeronautical Laboratory, June 13, 1942 to December 3, 1942.

22. Wind Tunnel Tests of a .3 Scale Model of the Republic P-47D Airplane, NACA Preliminary Data, Ames Aeronautical Laboratory, September to October, 1943.

CONFIDENTIAL
CLASSIFICATION cancelled

23. High Speed Wind Tunnel Tests of a 1/3 Scale Model of the XP-51 Airplane, NACA Preliminary Data, Ames Aeronautical Laboratory, July 20, 1944.

24. Wind Tunnel Tests of a 1/3 Scale Model of the North American P-51B, NACA Preliminary Data, Ames Aeronautical Laboratory, May, 1943 to July, 1943.

25. C. F. Hall — High Speed Longitudinal Control of the P-51B Airplane Calculated From Wind Tunnel Tests, NACA ACR, Ames Aeronautical Laboratory, March 20, 1944.

26. High Speed Wind Tunnel Tests of a 1/6 Scale Model of the Lockheed XP-58, NACA Preliminary Data, Ames Aeronautical Laboratory, July 1942 and December 1942.

27. High Speed Wind Tunnel Tests of a 3/16 Scale Model of the Douglas XSB2D-1 Airplane, NACA Preliminary Data, Ames Aeronautical Laboratory, July 1943 to April 1944.

28. Compressibility Studies on the XP-51 Airplane (Flight), NACA Preliminary Data, Langley Memorial Aeronautical Laboratory, March, 1944 to May, 1944.

29. Flight Tests of Republic P-47C Airplane, Wright Field Report (Unpublished), June 1943.

30. Republic Aviation Flight Test Report No. 105, Republic Aviation Corp., August, 1943.

31. R. E. Hage, and H. J. Heimer — **Effect of Compressibility on Drag and Terminal Velocity, Wright Field Memorandum Report, Eng. 51-4589-5, September 29, 1943**

CONFIDENTIAL
CLASSIFICATION cancelled

C. CONFIDENTIAL Cancelled

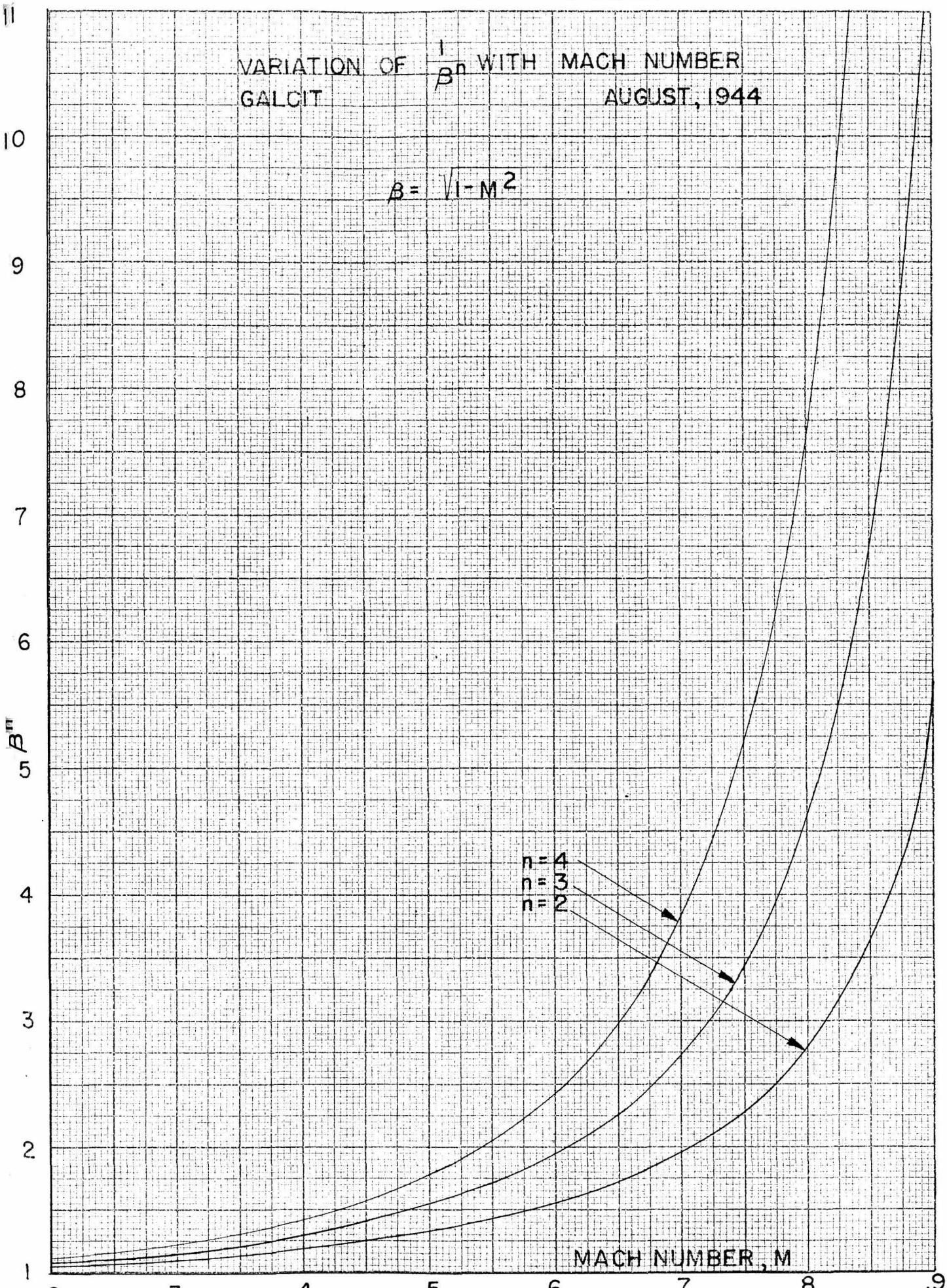

FIGURE 1

R/W/H 7/31/44

SKETCH OF STRUT AND GUARD DIMENSIONS
(REFERENCE 1, FIGURE 9)

GALCIT AUGUST, 1944

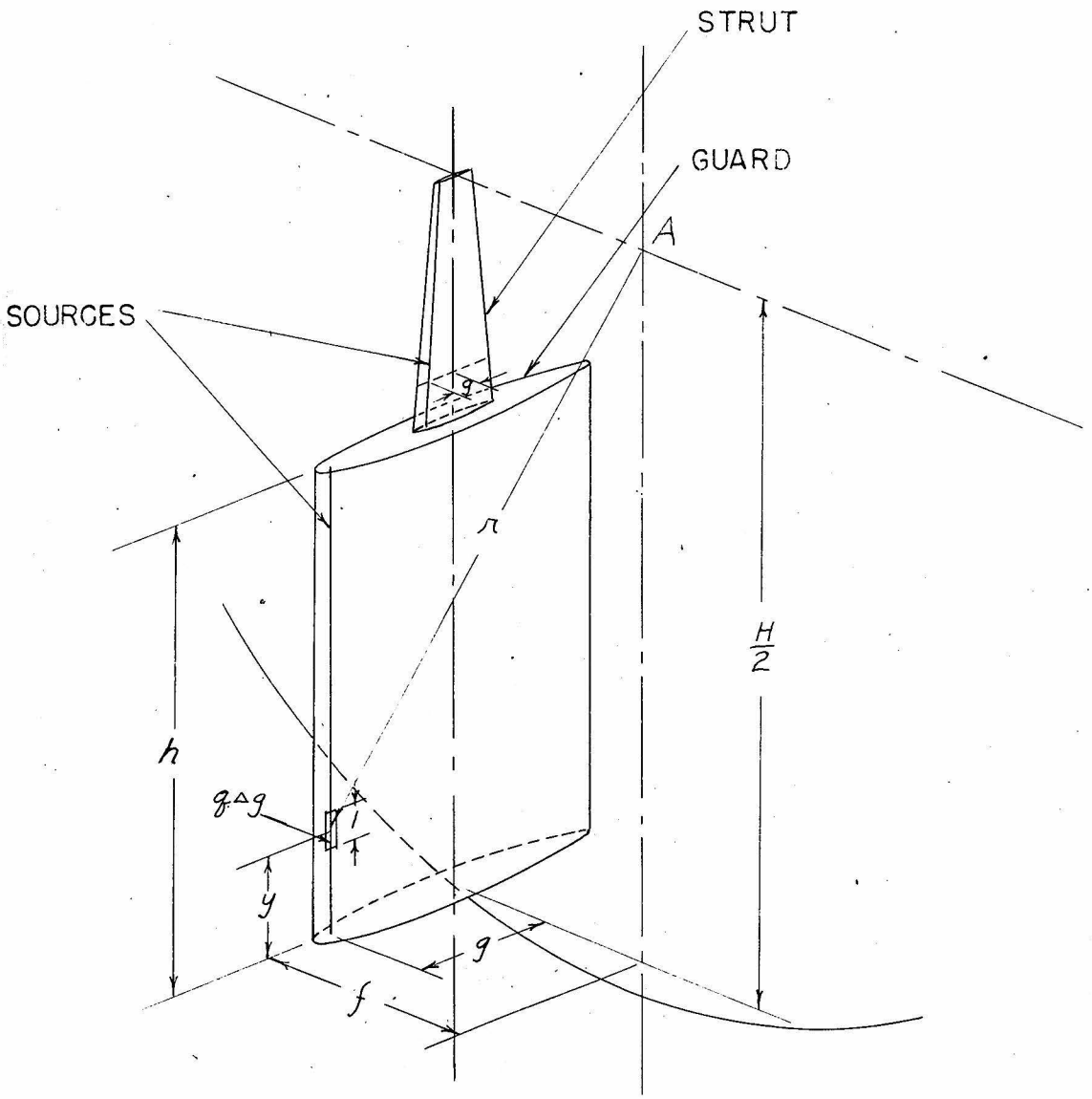

FIGURE 2

CLASSIFICATION cancelled

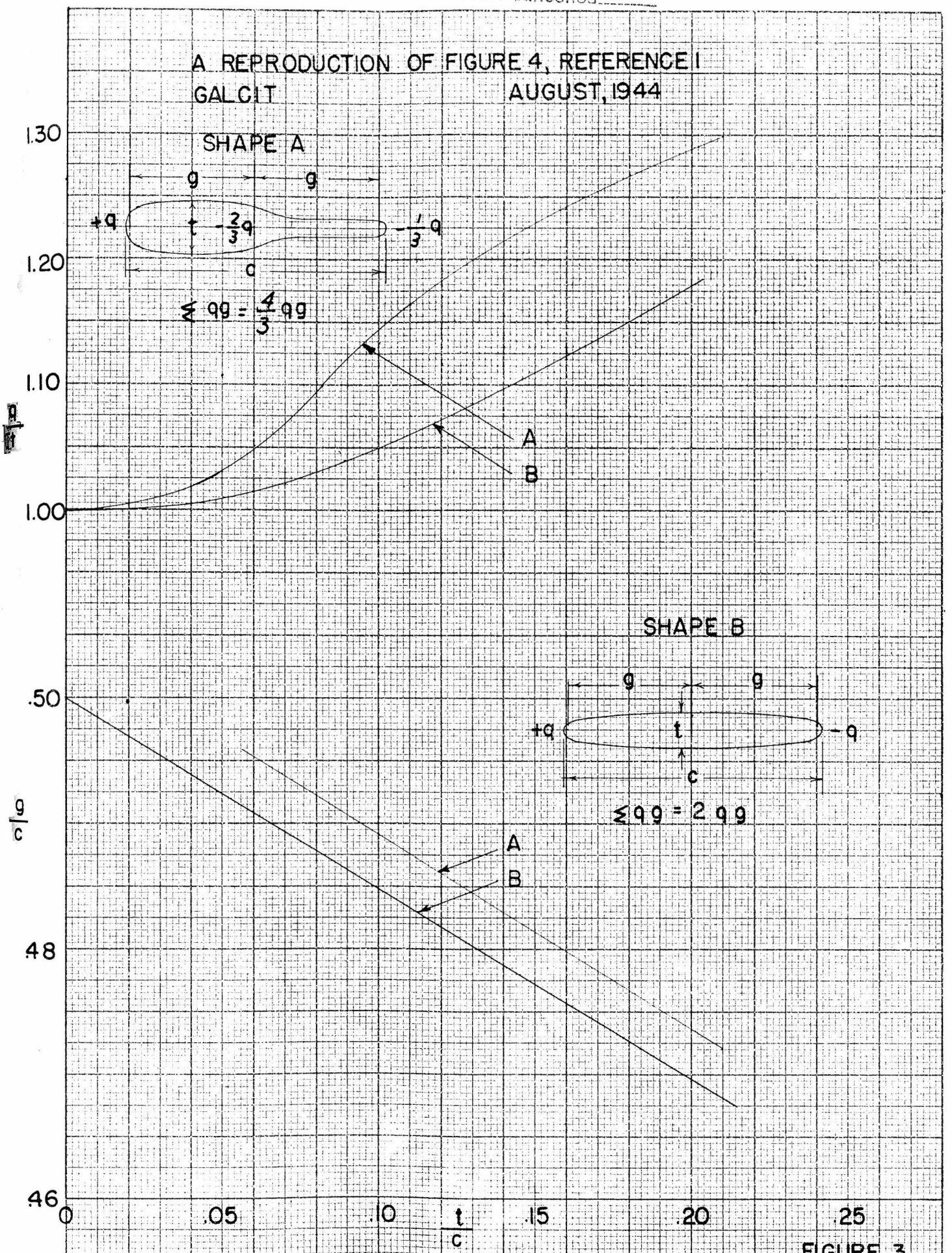

FIGURE 3

TWO DIMENSIONAL SHAPES

CONFIDENTIAL declassified

RWH 8/1/44

KEUFFEL & ESSER CO., N.Y. NO. 359-11L
10 × 10 to the ½ inch, 5th lines accented.
MADE IN U.S.A.

CLASSIFICATION CANCELLED
CONFIDENTIAL

DRAG RATIO AS A FUNCTION OF MACH NUMBER RATIO
B-29 COMPLETE MODEL REFERENCE 14
GALCIT AUGUST, 1944

	C_L	$(M_{CR})_C$	$(C_{D_{INC}})_C$
×	0	.611	.0251
⊙	.1	.604	.0248
△	.2	.597	.0253
□	.3	.590	.0267
▽	.4	.582	.0289
+	.5	.572	.0319

DRAG RATIO, $\left(\frac{C_D}{C_{D_{INC}}}\right)_C$

5.0
4.6
4.2
3.8
3.4
3.0
2.6
2.2
1.8
1.4
1.0

.5 .6 .7 .8 .9 1.0 1.1 1.2 1.3 1.4 1.5

MACH NUMBER RATIO, $\left(\frac{M}{M_{CR}}\right)_C$

FIGURE 4

CLASSIFICATION CANCELLED
CONFIDENTIAL

KEUFFEL & ESSER CO., N.Y. No. 389-11L
10 × 10 to the ½ inch, 5th line accented.
MADE IN U.S.A.

CLASSIFICATION cancelled
CONFIDENTIAL

DRAG RATIO AS A FUNCTION OF MACH NUMBER RATIO
C-69 COMPLETE MODEL REFERENCE 20
GALCIT AUGUST, 1944

	C_L	$(M_{CR})_C$	$(C_{D_{INC}})_C$
×	0	.632	.0220
○	.1	.625	.0208
△	.2	.607	.0212
□	.3	.583	.0226
▽	.4	.561	.0248
+	.5	.539	.0278

DRAG RATIO $\left(\frac{C_D}{C_{D_{INC}}}\right)_C$

5.8
5.4
5.0
4.6
4.2
3.8
3.4
3.0
2.6
2.2
1.8
1.4
1.0

.5 .6 .7 .8 .9 1.0 1.1 1.2 1.3 1.4 1.5

MACH NUMBER RATIO, $\left(\frac{M}{M_{CR}}\right)_C$

FIGURE 5

PWH 5/12/44

CONFIDENTIAL
Classification cancelled

KEUFFEL & ESSER CO., N. Y. No. 389-11L
10 × 10 to the ½ inch, 5th lines accented.
MADE IN U. S. A.

CLASSIFICATION cancelled
CONFIDENTIAL

DRAG RATIO AS A FUNCTION OF MACH NUMER RATIO
P-38 COMPLETE MODEL REFERENCE 21
GALCIT AUGUST, 1944

	C_L	$(M_{CR})_C$	$(C_{D_{INC}})_C$
×	0	.641	.0220
⊙	.1	.626	.0219
△	.2	.600	.0227
⊡	.3	.575	.0242
▽	.4	.550	.0270
+	.5	.525	.0307

DRAG RATIO, $\left(\frac{C_D}{C_{D_{INC}}}\right)_C$

5.8 5.4 5.0 4.6 4.2 3.8 3.4 3.0 2.6 2.2 1.8 1.4 1.0

.5 .6 .7 .8 .9 1.0 1.1 1.2 1.3 1.4 1.5

MACH NUMBER RATIO, $\left(\frac{M}{M_{CR}}\right)_C$

FIGURE 6

RWH 8/22/44

CLASSIFICATION cancelled
CONFIDENTIAL

KEUFFEL & ESSER CO., N.Y. No. 359-11L
10 × 10 to the ½ inch, 5th lines accented
MADE IN U.S.A.

CLASSIFICATION CONFIDENTIAL cancelled

DRAG RATIO AS A FUNCTION OF MACH NUMBER RATIO
P-47 COMPLETE MODEL — REFERENCE 22
GALCIT — AUGUST, 1944

	C_L	$(M_{CR})_C$	$(C_{D_{INC}})_C$
×	0	.691	.0176
⊙	.1	.664	.0176
△	.2	.627	.0187
□	.3	.588	.0208
▽	.4	.544	.0246
+	.5	.494	.0298

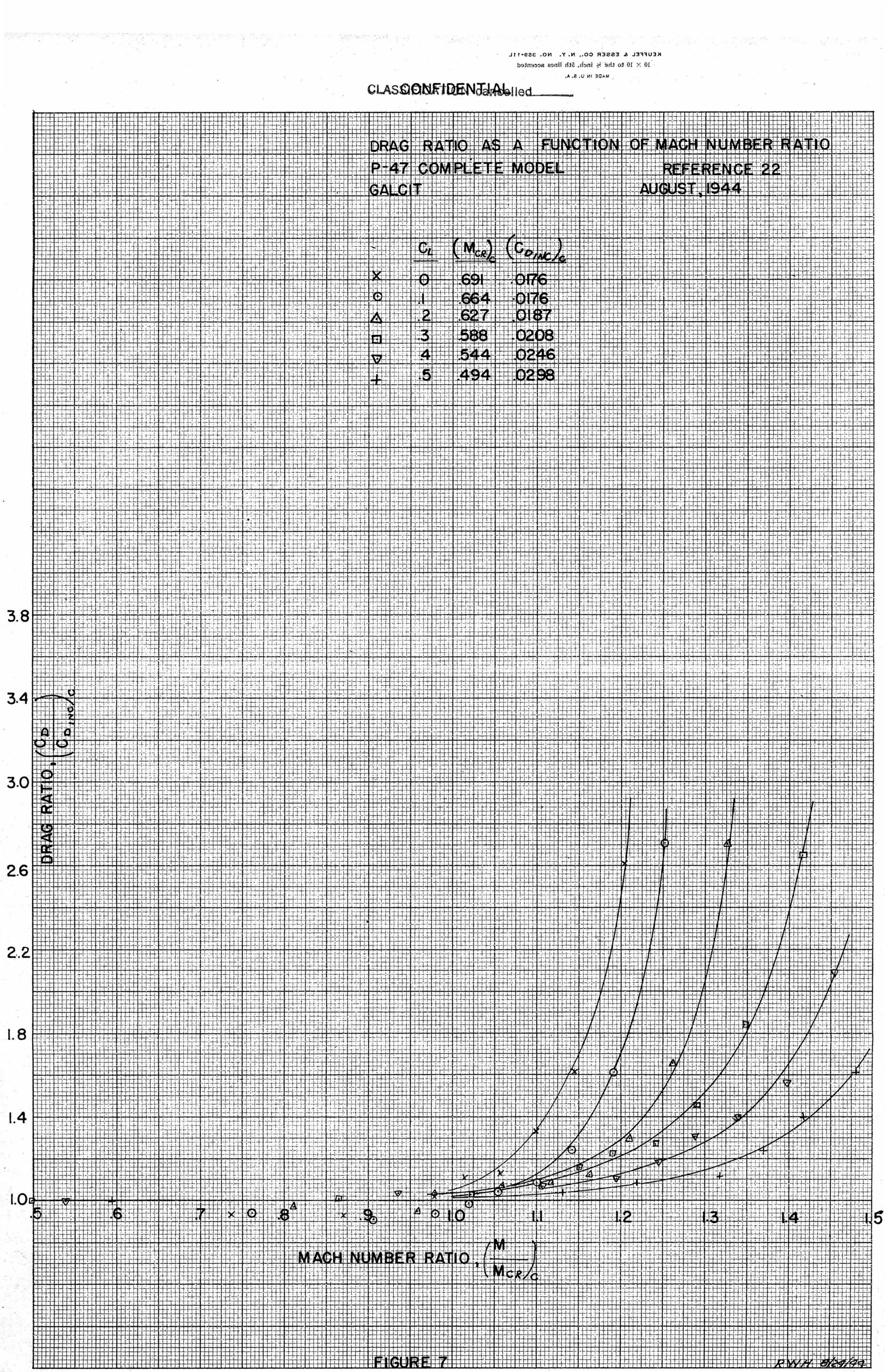

FIGURE 7

RWH 8/24/44

CONFIDENTIAL cancelled

FIGURE 7

KEUFFEL & ESSER CO., N. Y. No. 389-11L
10 × 10 to the ½ inch, 5th lines accented.
MADE IN U.S.A.

CONFIDENTIAL
CLASSIFICATION cancelled

DRAG RATIO AS A FUNCTION OF MACH NUMBER RATIO
P-58 COMPLETE MODEL WITH NACA 230XX WING, REFERENCE 26
GALCIT AUGUST, 1944

	C_L	$(M_{CR})_C$	$(C_{D_{INC.}})_C$
×	0	.644	.0204
⊙	.1	.627	.0201
△	.2	.603	.0210
□	.3	.583	.0228
▽	.4	.558	.0257
+	.5	.537	.0291

DRAG RATIO, $\left(\frac{C_D}{C_{D_{INC.}}}\right)_C$

5.0
4.6
4.2
3.8
3.4
3.0
2.6
2.2
1.8
1.4
1.0

.5 .6 .7 .8 .9 1.0 1.1 1.2 1.3 1.4 1.5

MACH NUMBER RATIO, $\left(\frac{M}{M_{CR}}\right)_C$

FIGURE 8

R W H 8/23/44

CONFIDENTIAL
CLASSIFICATION cancelled

FIGURE 8

KEUFFEL & ESSER CO., N.Y. NO. 389-11L
10 × 10 to the ½ inch, 5th lines accented
MADE IN U.S.A.

CLASSIFICATION cancelled

CONFIDENTIAL

CLASSIFICATION cancelled

DRAG RATIO AS A FUNCTION OF MACH NUMBER RATIO
B-42 COMPLETE MODEL REFERENCE 19
GALCIT AUGUST, 1944

	C_L	$(M_{CR})_C$	$(C_{D_{INC}})_C$
×	0	.685	.0162
⊙	.1	.676	.0160
△	.2	.667	.0170
□	.3	.659	.0191
▽	.4	.651	.0219
+	.5	.642	.0254

DRAG RATIO, $\left(\frac{C_D}{C_{D_{INC}}}\right)_C$

5.8
5.4
5.0
4.6
4.2
3.8
3.4
3.0
2.6
2.2
1.8
1.4
1.0

.4 .5 .6 .7 .8 .9 1.0 1.1 1.2 1.3 1.4

MACH NUMBER RATIO, $\left(\frac{M}{M_{CR}}\right)_C$

FIGURE 9

RWH 8/21/44

CONFIDENTIAL

CLASSIFICATION cancelled

FIGURE 9

KEUFFEL & ESSER CO., N.Y. No. 359-11L
10 × 10 to the ½ inch, 5th lines accented.
MADE IN U.S.A.

CLASSIFIED CONFIDENTIAL

DRAG RATIO AS A FUNCTION OF MACH NUMBER RATIO
XP-51 COMPLETE MODEL REFERENCE 23
GALCIT AUGUST, 1944

	C_L	$(M_{CR})_C$	$(C_{D_{INC}})_C$
X	0	.705	.0173
⊙	.1	.694	.0173
△	.2	.682	.0189
□	.3	.669	.0216
▽	.4	.658	.0256
+	.5	.643	.0305

DRAG RATIO, $\left(\frac{C_D}{C_{D_{INC}}}\right)_C$

5.0
4.6
4.2
3.8
3.4
3.0
2.6
2.2
1.8
1.4
1.0

.5 .6 .7 .8 .9 1.0 1.1 1.2 1.3 1.4 1.5

MACH NUMBER RATIO, $\left(\frac{M}{M_{CR}}\right)_C$

FIGURE 10

RWH 8/22/45

CLASSIFIED CONFIDENTIAL

KEUFFEL & ESSER CO., N. Y. No. 389-11L
10 × 10 to the ½ inch, 5th lines accented.
MADE IN U. S. A.

CLASSIFICATION cancelled
CONFIDENTIAL

DRAG RATIO AS A FUNCTION OF MACH NUMBER RATIO
P-51B COMPLETE MODEL, REFERENCE 25
GALCIT AUGUST, 1944

	C_L	$(M_{cr})_c$	$(C_{D_{inc}})_c$
X	0	.698	.0177
⊙	1	.685	.0181
△	2	.677	.0196
□	3	.666	.0225
▽	4	.653	.0264
+	5	.635	.0316

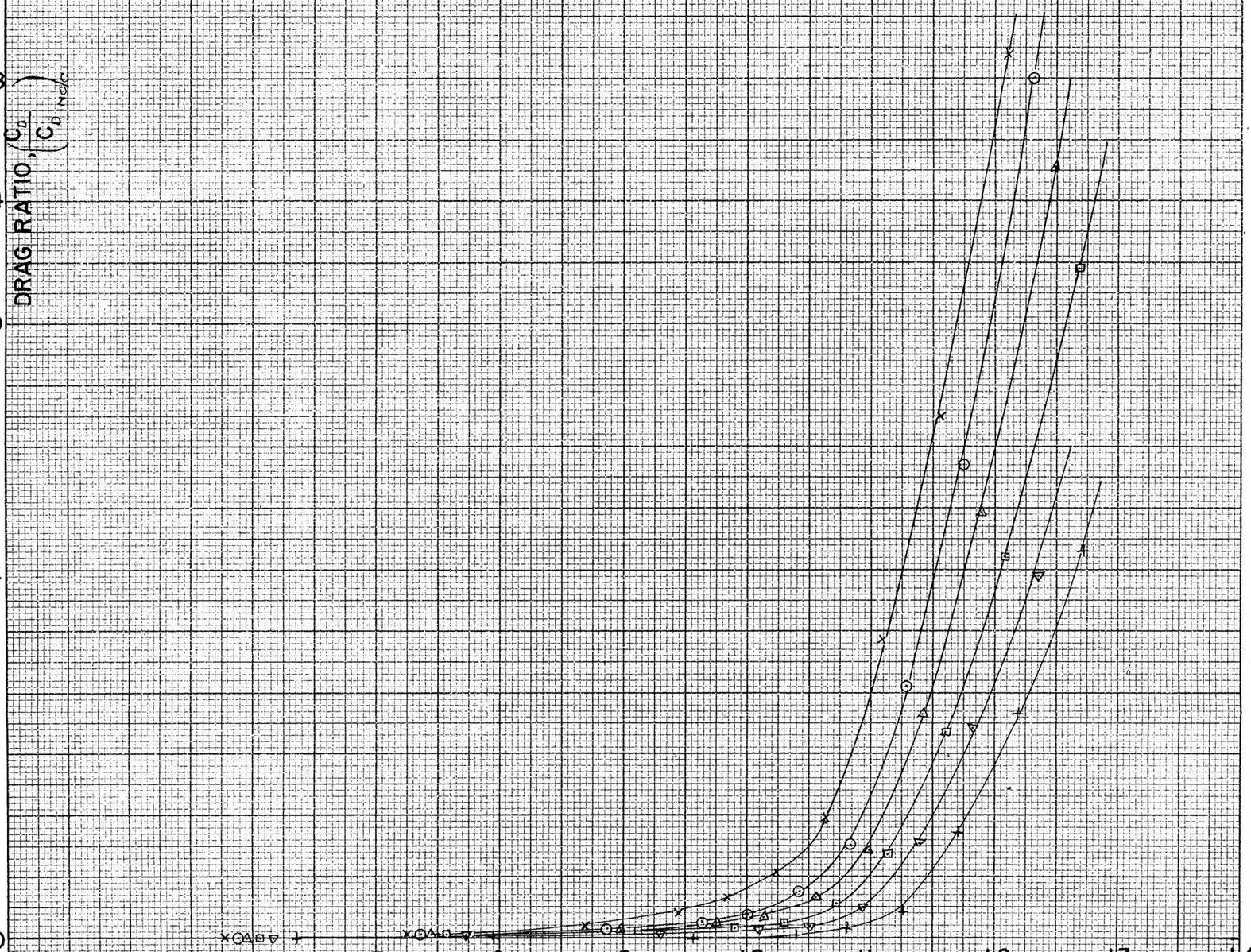

FIGURE 11

RWH 8/2/44

CONFIDENTIAL
CLASSIFICATION cancelled

CLASSIFICATION cancelled

CONFIDENTIAL

DRAG RATIO AS A FUNCTION OF MACH NUMBER RATIO

P-58 COMPLETE MODEL WITH NACA 66 SERIES WING, REFERENCE 26

GALCIT AUGUST, 1944

	C_L	$(M_{CR})_C$	$(C_{D_{INC}})_C$
X	0	.698	.0188
⊙	.1	.694	.0191
△	.2	.685	.0199
□	.3	.670	.0221
▽	.4	.655	.0254
+	.5	.635	.0302

DRAG RATIO, $\left(\frac{C_D}{C_{D_{INC}}}\right)_C$

5.0
4.6
4.2
3.8
3.4
3.0
2.6
2.2
1.8
1.4
1.0

.5 .6 .7 .8 .9 1.0 1.1 1.2 1.3 1.4 1.5

MACH NUMBER RATIO, $\left(\frac{M}{M_{CR_C}}\right)$

FIGURE 12

RWH 8/23/94

FIGURE 12

CONFIDENTIAL

CLASSIFICATION cancelled

CONFIDENTIAL
CLASSIFICATION cancelled

DRAG RATIO AS A FUNCTION OF MACH NUMBER RATIO
X SB 2D-1 COMPLETE MODEL REFERENCE 27
GALCIT AUGUST, 1944

	C_L	$(M_{CR})_C$	$(C_{D_{INC.}})_C$
X	0	.674	.0194
⊙	.1	.666	.0197
△	.2	.659	.0211
□	.3	.653	.0246
▽	.4	.646	.0294
+	.5	.638	.0361

DRAG RATIO, $\left(\frac{C_D}{C_{D_{INC.}}}\right)_C$

5.0
4.6
4.2
3.8
3.4
3.0
2.6
2.2
1.8
1.4
1.0

.4 .5 .6 .7 .8 .9 1.0 1.1 1.2 1.3 1.4

MACH NUMBER RATIO, $\left(\frac{M}{M_{CR}}\right)_C$

FIGURE 13

RWH 8/2/44

CONFIDENTIAL
CLASSIFICATION cancelled

KEUFFEL & ESSER CO., N. Y. No. 389-11L
10 × 10 to the ½ inch, 5th lines accented.
MADE IN U.S.A.

CONFIDENTIAL
Classification Cancelled

DRAG RATIO AS A FUNCTION OF MACH NUMBER RATIO
MODELS WITH CONVENTIONAL, LOW SPEED AIRFOILS
GALCIT AUGUST, 1944

$C_L = 0$

		$(M_{CR})_c$	$(C_{D_{INC}})_c$
X	B-29	.611	0251
⊙	C-69	632	0220
△	P-38	641	0220
⊡	P-47	691	0176
▽	P-58	644	0204

DRAG RATIO, $\left(\frac{C}{C_{D_{INC}}}\right)_c$

5.4
5.0
4.6
4.2
3.8
3.4
3.0
2.6
2.2
1.8
1.4
1.0

.4 .5 .6 .7 .8 .9 1.0 1.1 1.2 1.3 1.4

MACH NUMBER RATIO, $\left(\frac{M}{(M_{CR})_c}\right)$

FIGURE 14

RWH 8/24/44

CONFIDENTIAL
Classification Cancelled

CONFIDENTIAL
CLASSIFICATION cancelled

DRAG RATIO AS A FUNCTION OF MACH NUMBER RATIO
MODELS WITH CONVENTIONAL, LOW SPEED AIRFOILS
GALCIT AUGUST, 1944

$C_L = .1$

		$(M_{CR})_c$	$(C_{D_{INC}})_c$
×	B-29	.604	.0248
⊙	C-69	.625	.0208
△	P-38	.626	.0219
□	P-47	.664	.0176
▽	P-58	.627	.0201

DRAG RATIO, $\left(\frac{C_D}{C_{D_{INC}}}\right)_c$

5.4
5.0
4.6
4.2
3.8
3.4
3.0
2.6
2.2
1.8
1.4
1.0

.5 .6 .7 .8 .9 1.0 1.1 1.2 1.3 1.4 1.5

MACH NUMBER RATIO, $\left(\frac{M}{M_{CR}}\right)_c$

FIGURE 15

FIGURE 15

CONFIDENTIAL
CLASSIFICATION cancelled

KEUFFEL & ESSER CO., N. Y. No. 359-11L
10 × 10 to the ½ inch, 5th lines accented.
MADE IN U.S.A.

CONFIDENTIAL

DRAG RATIO AS A FUNCTION OF MACH NUMBER RATIO
MODELS WITH CONVENTIONAL, LOW SPEED AIRFOILS
GALCIT AUGUST, 1944

$C_L = 2$

		$(M_{CR})_C$	$(C_{D,INC})_C$
X	B-29	.597	.0253
⊙	C-69	.607	.0212
△	P-38	.600	.0227
□	P-47	.627	.0187
▽	P-58	.603	.0210

DRAG RATIO, $\left(\frac{C_D}{C_{D,INC}}\right)_C$

5.8
5.4
5.0
4.6
4.2
3.8
3.4
3.0
2.6
2.2
1.8
1.4
1.0

.5 .6 .7 .8 .9 1.0 1.1 1.2 1.3 1.4 1.5

MACH NUMBER RATIO, $\left(\frac{M}{M_{CR}}\right)_C$

FIGURE 16

RWH 8/29/44

CLASSIFICATION cancelled
CONFIDENTIAL

KEUFFEL & ESSER CO., N.Y. NO. 389-11L
10 × 10 to the ½ inch, 5th linge accepted.
MADE IN U.S.A.

CLASSIFICATION CANCELLED
CONFIDENTIAL

DRAG RATIO AS A FUNCTION OF MACH NUMBER RATIO
MODELS WITH CONVENTIONAL, LOW SPEED AIRFOILS
GALCIT AUGUST, 1944

$C_L = .3$

		$(M_{CR})_C$	$(C_{D_{INC}})_C$
×	B-29	.590	.0267
⊙	C-69	.583	.0226
△	P-38	.575	.0242
□	P-47	.588	.0208
▽	P-58	.583	.0228

DRAG RATIO, $\left(\frac{C_D}{C_{D_{INC}}}\right)_C$

5.8
5.4
5.0
4.6
4.2
3.8
3.4
3.0
2.6
2.2
1.8
1.4
1.0

.5 .6 .7 .8 .9 1.0 1.1 1.2 1.3 1.4 1.5

MACH NUMBER RATIO, $\left(\frac{M}{M_{CR}}\right)_C$

FIGURE 17

RWH 8/20/44

CLASSIFICATION CANCELLED
CONFIDENTIAL

DRAG RATIO AS A FUNCTION OF MACH NUMBER RATIO
MODELS WITH CONVENTIONAL, LOW SPEED AIRFOILS
GALCIT AUGUST, 1944

$C_L = .4$

		$(M_{CR})_c$	$(C_{D_{INC}})_c$
X	B-29	.582	.0289
⊙	C-69	.561	.0248
△	P-38	.550	.0270
⊡	P-47	.544	.0246
▽	P-58	.558	.0257

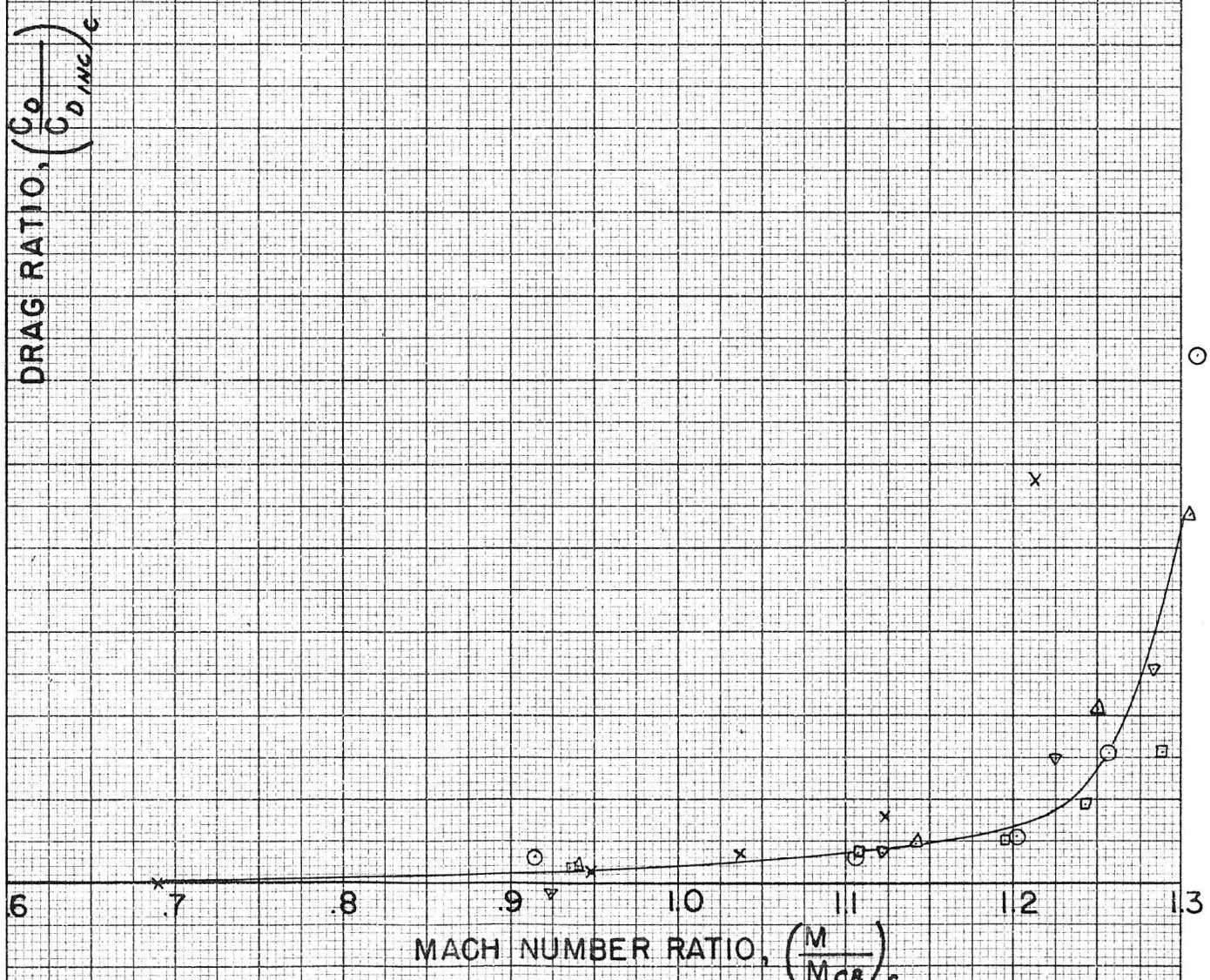

FIGURE 18

RWH 8/29/44

DRAG RATIO AS A FUNCTION OF MACH NUMBER RATIO
MODELS WITH CONVENTIONAL, LOW SPEED AIRFOILS
GALCIT AUGUST, 1944

$C_L = .5$

		$(M_{CR})_c$	$(C_{D_{INC}})_c$
×	B-29	.572	.0319
⊙	C-69	.539	.0278
△	P-38	.525	.0307
⊡	P-47	494	.0298
▽	P-58	.537	.0291

DRAG RATIO, $\left(\frac{C_D}{C_{D_{INC}}}\right)_c$

3.0
2.6
2.2
1.8
1.4
1.0

.6 .7 .8 .9 1.0 1.1 1.2 1.3

MACH NUMBER RATIO, $\left(\frac{M}{M_{CR}}\right)_c$

FIGURE 19

RWH 8/24/44

KEUFFEL & ESSER CO., N. Y. No. 359-11L
10 × 10 to the ½ inch, 5th lines accented.
MADE IN U. S. A.

CLASSIFICATION cancelled

CONFIDENTIAL

DRAG RATIO AS A FUNCTION OF MACH NUMBER RATIO
MODELS WITH HIGH SPEED, LOW DRAG AIRFOILS
GALCIT AUGUST, 1944

$C_L = 0$

		$(M_{CR})_c$	$(C_{D_{INC}})_c$
×	B-42	.685	.0162
⊙	XP-51	.705	.0173
△	P-51B	.698	.0177
⊡	P-58	.698	.0188
▽	XSB2D1	.674	.0194

DRAG RATIO, $\left(\frac{C_D}{C_{D_{INC}}}\right)_c$

5.8
5.4
5.0
4.6
4.2
3.8
3.4
3.0
2.6
2.2
1.8
1.4
1.0

.4 .5 .6 .7 .8 .9 1.0 1.1 1.2 1.3 1.4

MACH NUMBER RATIO, $\left(\frac{M}{M_{CR_c}}\right)$

FIGURE 20

RWH 8/23/44

CONFIDENTIAL

CLASSIFICATION cancelled

KEUFFEL & ESSER CO., N. Y. No. 389-11L
10 × 10 to the ½ inch, 5th lines accented.
MADE IN U. S. A.

CONFIDENTIAL
CLASSIFICATION cancelled

DRAG RATIO AS A FUNCTION OF MACH NUMBER RATIO
MODELS WITH HIGH SPEED, LOW DRAG AIRFOILS
GALCIT · AUGUST, 1944

$C_L = .1$

		$(M_{cr})_c$	$(C_{D\,inc})_c$
×	B-42	.676	.0160
⊙	XP-51	.694	.0173
△	P-51B	.685	.0181
⊡	P-58	.694	.0191
▽	XSB2D-1	.666	.0197

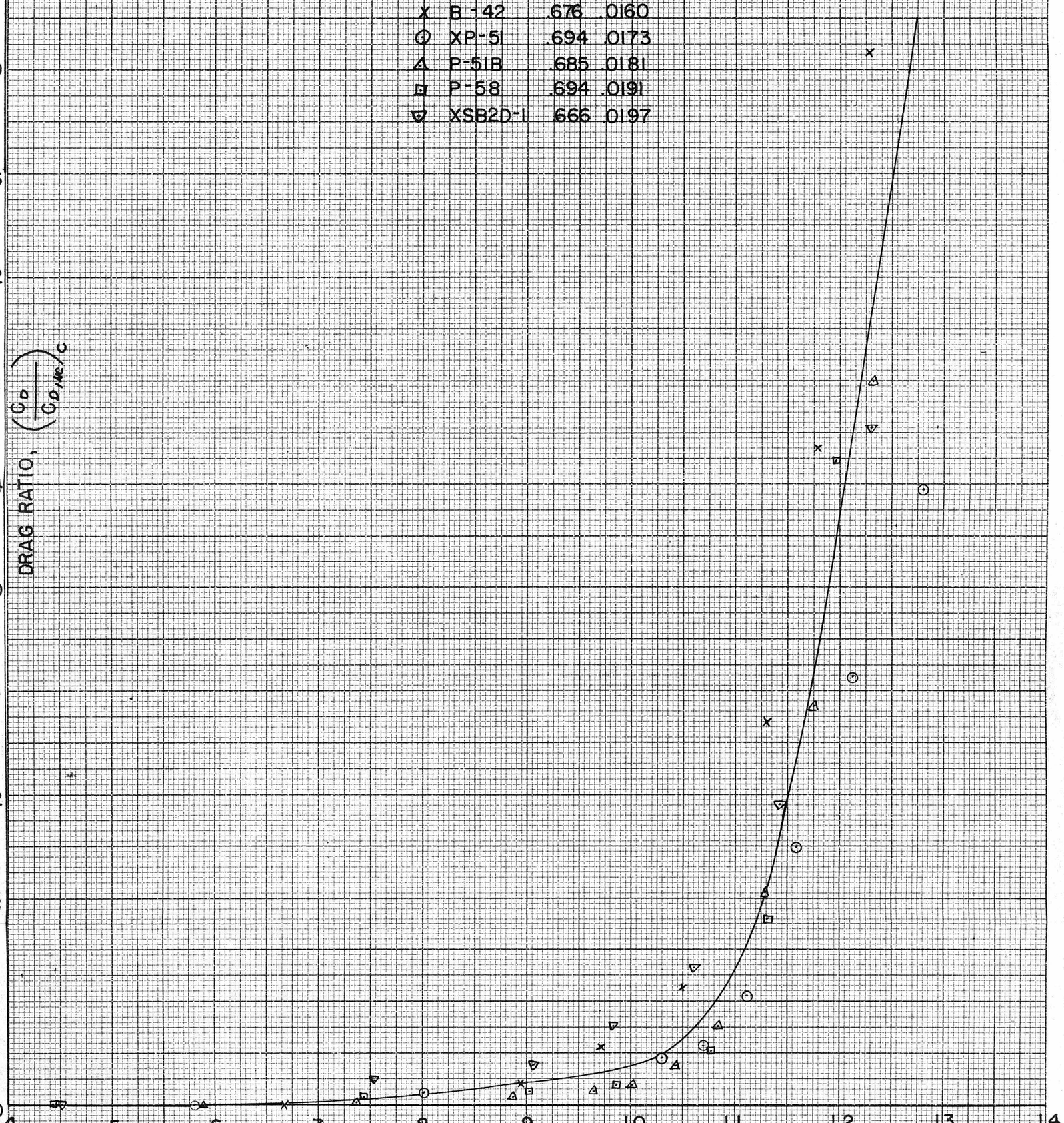

FIGURE 21

RWH 8/20/44

CONFIDENTIAL
CLASSIFICATION cancelled

KEUFFEL & ESSER CO., N. Y. No. 359-11L
10 × 10 to the ½ inch, 6th lines accented
MADE IN U. S. A.

CLASSIFICATION CONFIDENTIAL

DRAG RATIO AS A FUNCTION OF MACH NUMBER RATIO
MODELS WITH HIGH SPEED, LOW DRAG AIRFOILS
GALCIT AUGUST, 1944

$C_L = .2$

		$(M_{cr})_c$	$(C_{D,INC})_c$
X	B-42	.667	.0170
⊙	XP-51	.682	.0189
△	P-51B	.677	.0196
⊡	P-58	.685	.0199
▽	XSB2D-1	.659	.0211

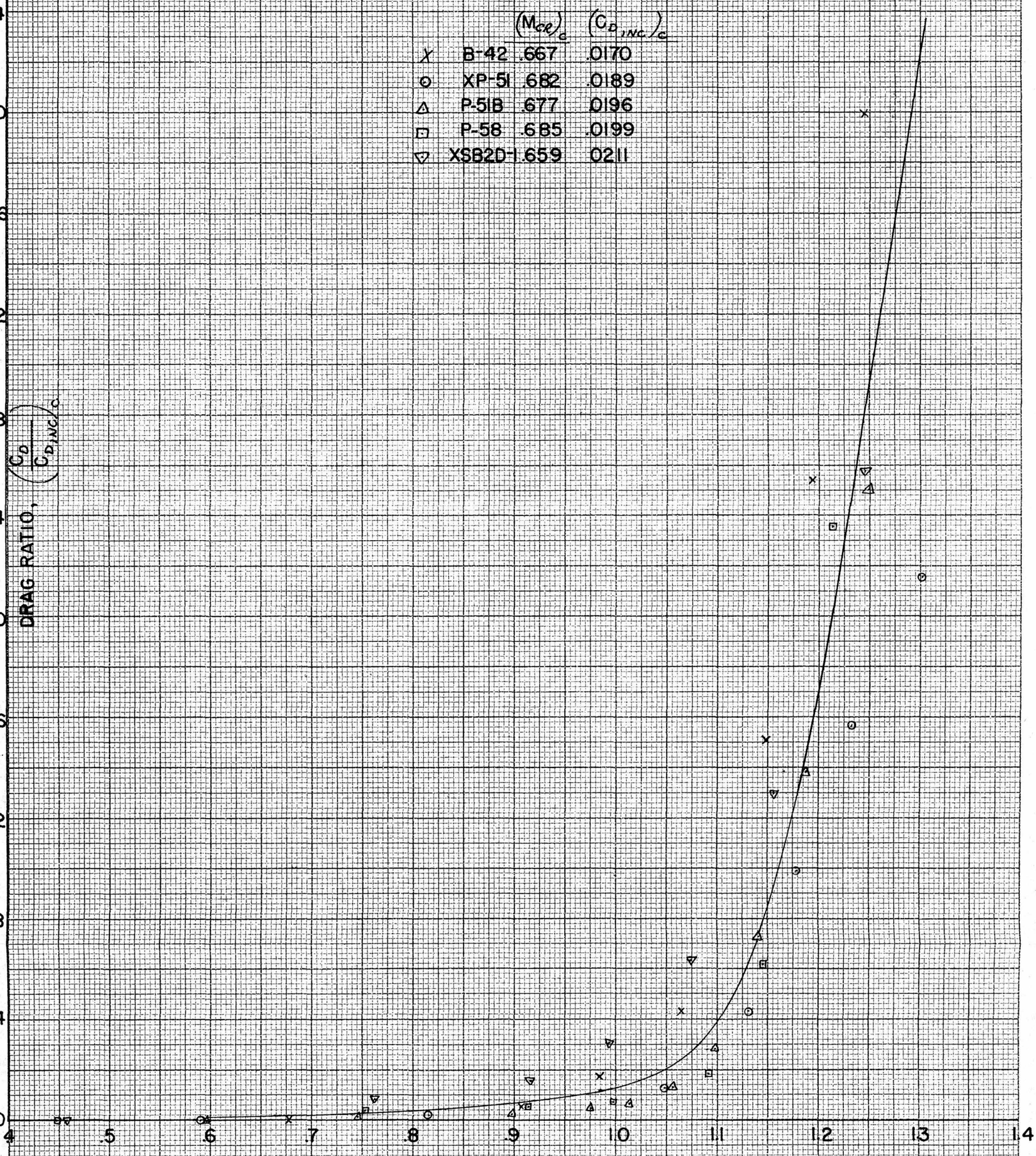

FIGURE 22

RWH 8/29/44

CLASSIFICATION CONFIDENTIAL Declassified

CLASSIFICATION CANCELLED
CONFIDENTIAL

DRAG RATIO AS A FUNCTION OF MACH NUMBER RATIO
MODELS WITH HIGH SPEED, LOW DRAG AIRFOILS
GALCIT AUGUST, 1944

$C_L = .3$

		$(M_{CR})_c$	$(C_{D,INC})_c$
×	B-42	.659	0191
⊙	XP-51	669	0216
△	P-51B	666	.0225
⊡	P-58	670	.0221
▽	XSB2D-1	653	.0246

DRAG RATIO, $\left(\frac{C_D}{C_{D,INC}}\right)_c$

5.4
5.0
4.6
4.2
3.8
3.4
3.0
2.6
2.2
1.8
1.4
1.0

.4 .5 .6 .7 .8 .9 1.0 1.1 1.2 1.3 1.4

MACH NUMBER RATIO, $\left(\frac{M}{M_{CR}}\right)_c$

FIGURE 23

R.W.H. Stoke

CLASSIFICATION CANCELLED
CONFIDENTIAL

DRAG RATIO AS A FUNCTION OF MACH NUMBER RATIO
MODELS WITH HIGH SPEED, LOW DRAG AIRFOILS
GALCIT AUGUST, 1944

		$C_L = .4$ $(M_{CR})_c$	$(C_{D_{INC}})_c$
X	B-42	.651	.0219
⊙	XP-51	.658	.0256
△	P-51B	.653	.0264
□	P-58	.655	.0254
▽	XSB2D-1	.646	.0294

DRAG RATIO, $\left(\frac{C_D}{C_{D_{INC}}}\right)_c$

3.8
3.4
3.0
2.6
2.2
1.8
1.4
1.0

.6 .7 .8 .9 1.0 1.1 1.2 1.3

MACH NUMBER RATIO, $\left(\frac{M}{M_{CR}}\right)_c$

FIGURE 24

RWH 8/30/44

DRAG RATIO AS A FUNCTION OF MACH NUMBER RATIO
MODELS WITH HIGH SPEED, LOW DRAG AIRFOILS
GALCIT AUGUST, 1944

$C_L = .5$

		$(M_{CR})_c$	$(C_{D_{INC}})_c$
X	B-42	.642	.0254
⊙	XP-51	.643	.0305
△	P-51B	.635	.0316
⊡	P-58	.635	.0302
▽	XSB2D-1	.638	.0361

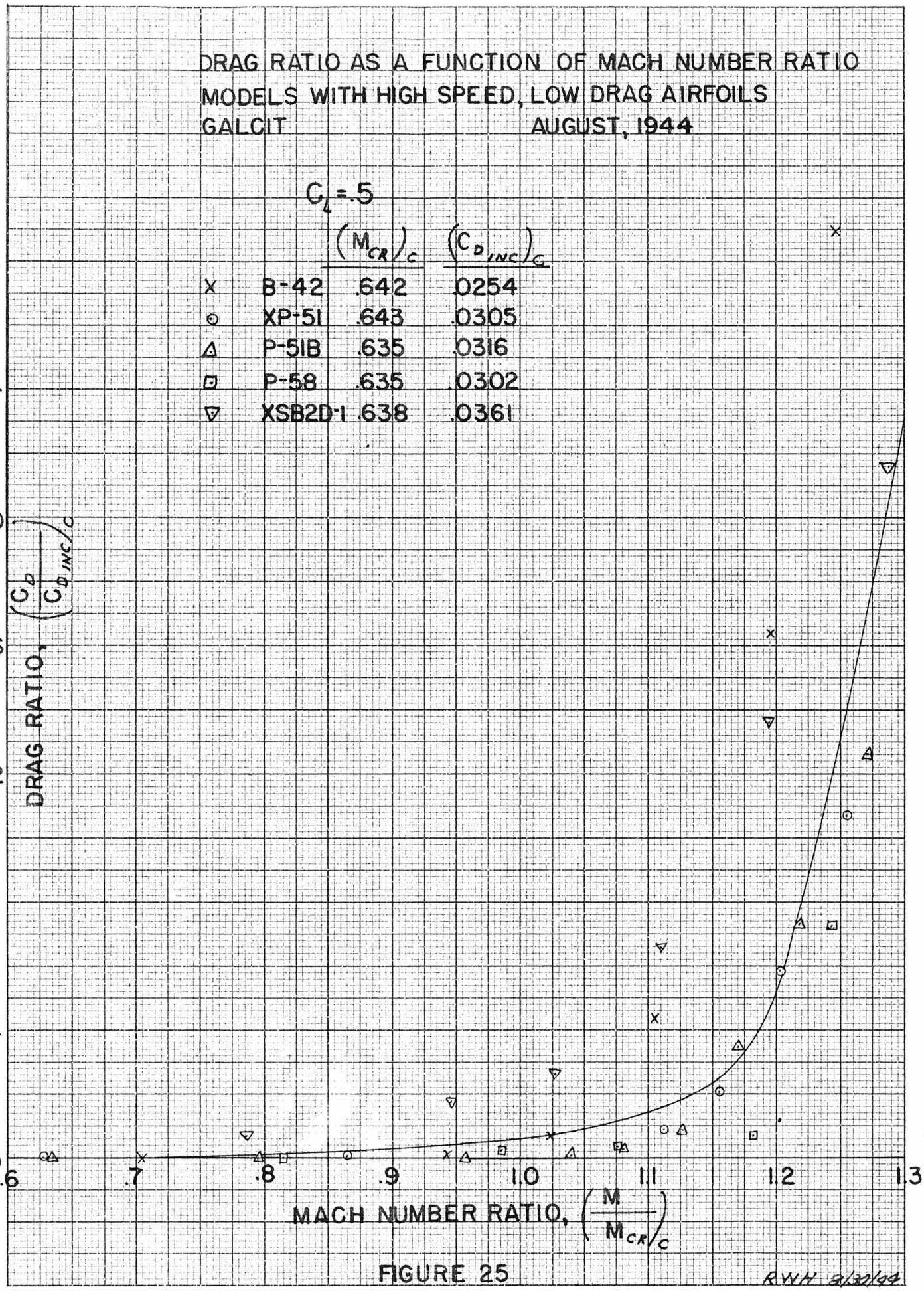

FIGURE 25

RWH 8/30/44

CONFIDENTIAL
Classification cancelled

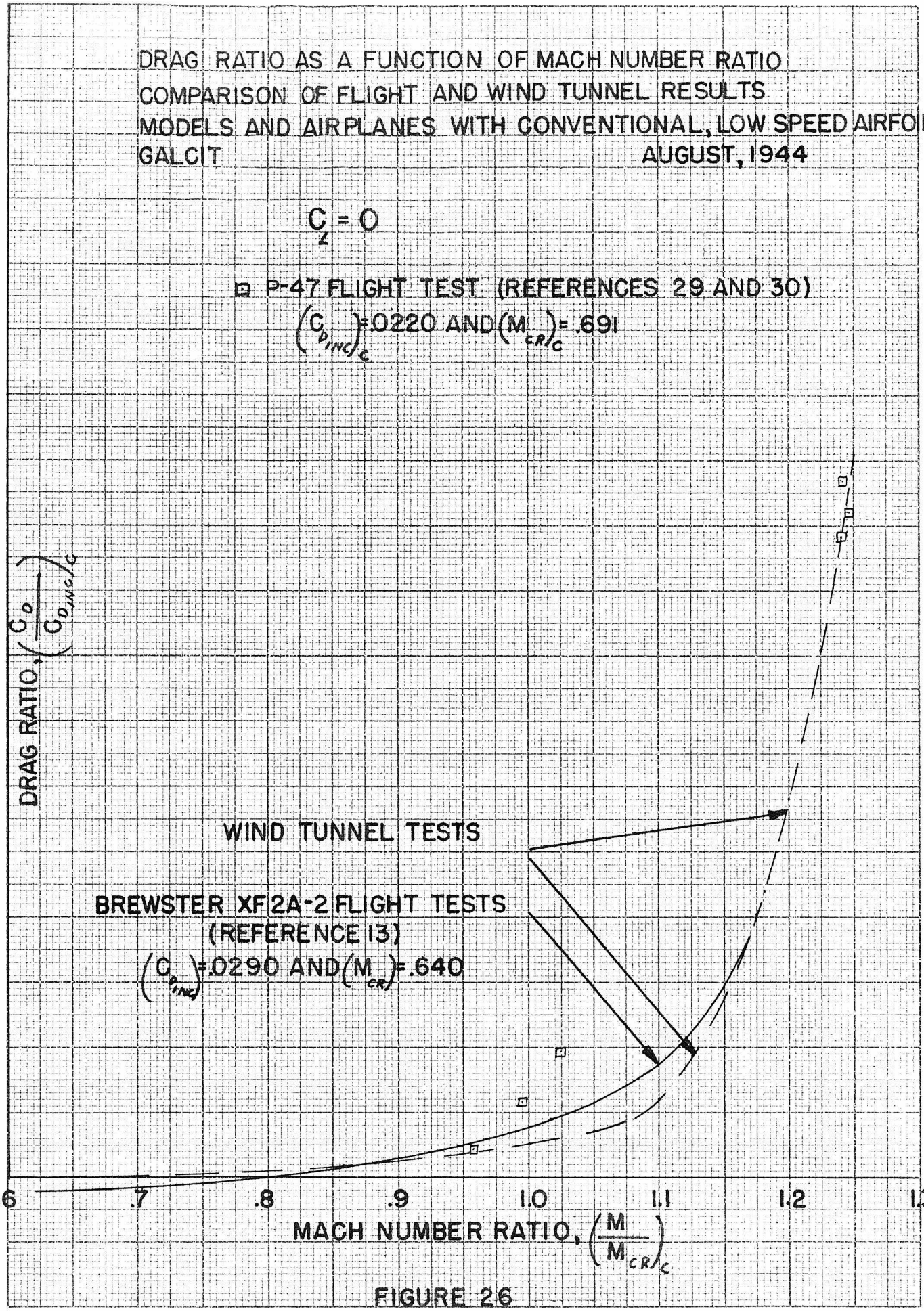

FIGURE 26

CONFIDENTIAL
Classification cancelled

RWH 8/20/44

10 × 10 to the in. 5th lines accented
MADE IN U.S.A.

CONFIDENTIAL
CLASSIFICATION cancelled

DRAG RATIO AS A FUNCTION OF MACH NUMBER RATIO

SUMMARY OF MEAN VARIATION AT EACH LIFT COEFFICIENT

MODELS WITH CONVENTIONAL, LOW SPEED AIRFOILS

GALCIT AUGUST, 1944

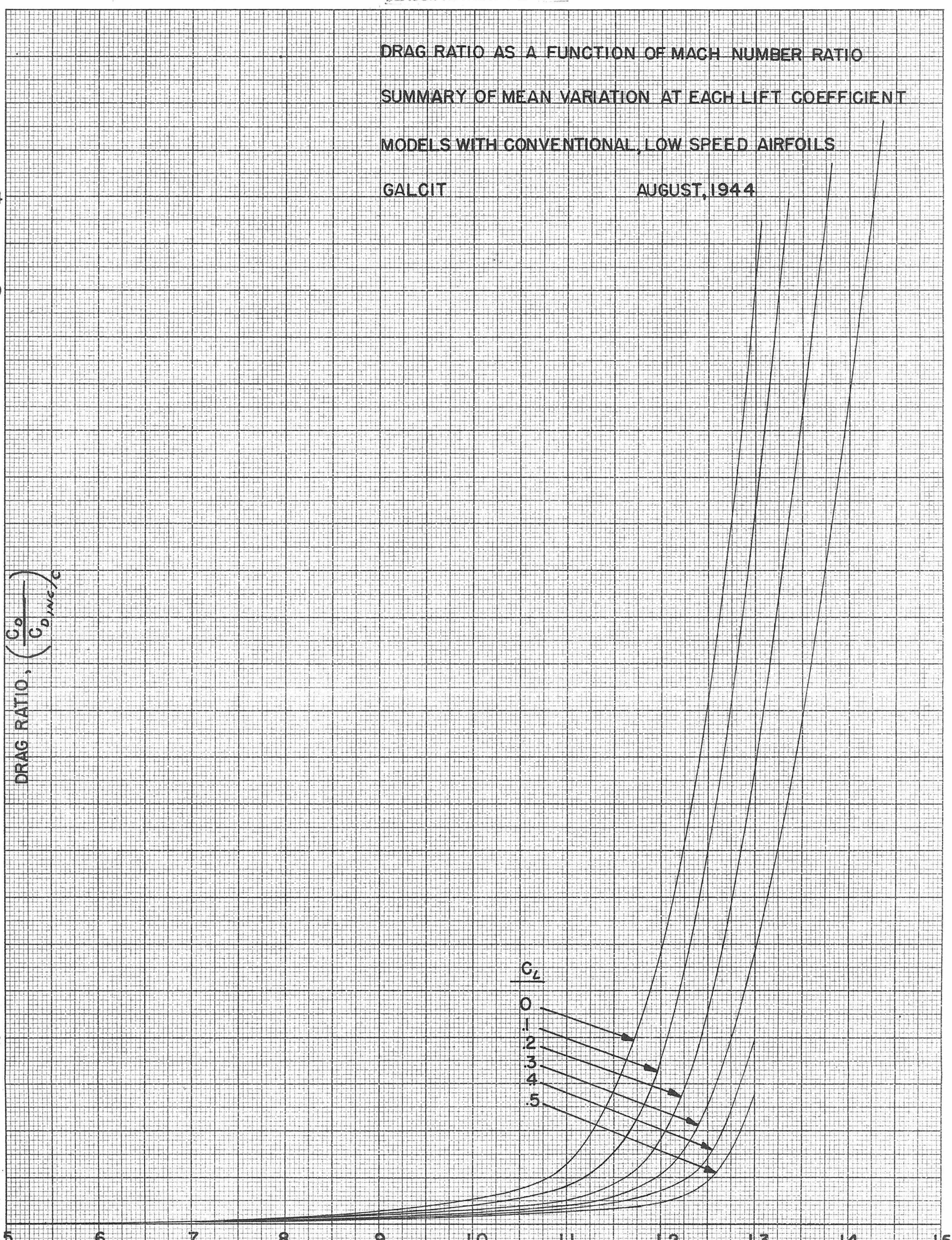

FIGURE 27

H.J.H. 9/10/44

CLASSIFICATION cancelled
CONFIDENTIAL

KEUFFEL & ESSER CO., N.Y. No. 359-11L
10 × 10 to the ½ inch, 5th lines accented
MADE IN U.S.A.

CLASSIFICATION CANCELLED

CONFIDENTIAL

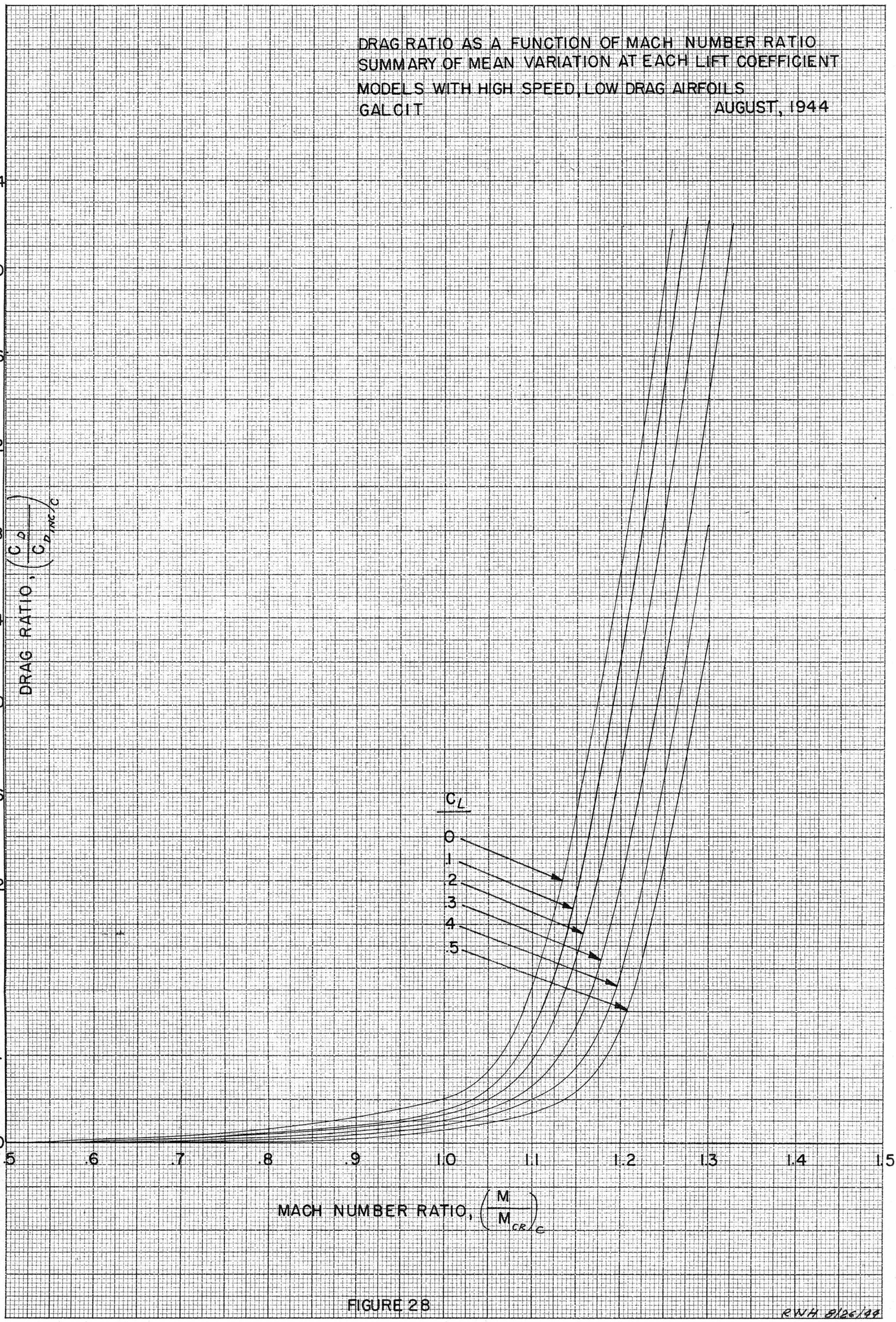

FIGURE 28

RWH 8/26/44

CLASSIFICATION CANCELLED

CONFIDENTIAL

CLASSIFICATION cancelled

APPENDIX I

C-69 Blocking Corrections

A. Model Wing Solid Blocking (Three-dimensional)

$$\epsilon_{C_A} = \frac{1.2\ sct}{A^{\frac{3}{2}}\ \beta^3} = \frac{.0003}{\beta^3}$$

B. Model Fuselage Solid Blocking

$$\epsilon_{C_B} = \frac{.96 \times .45\ \ell\ d^2}{A^{\frac{3}{2}}\ \beta^4} = \frac{.0006}{\beta^4}$$

C. Front Struts and Strut Guards Solid Blocking

1. $\epsilon_{c_{c_1}} = K_1 \times \frac{tc}{\beta^3} = \frac{.0110}{\beta^3}$ (Guards - Pg. 71)

2. $\epsilon_{c_{c_2}} = K_2 \times \frac{tc}{\beta^3} = \frac{.0020}{\beta^3}$ (Struts - Pg. 72)

$$\epsilon_{c_c} = \frac{.0130}{\beta^3}$$

D. Model Wake

$$\epsilon_{c_D} = 1/4\ \frac{C_{D_p} \cdot S}{A\beta^3} = \frac{.0108\ C_{D_p}}{\beta^3}$$

E. Front Strut Guard Wake

$$\epsilon_{c_E} = 1/4\ \frac{C_{D_p} \cdot S}{A\beta^3}$$

F. Rear Strut Guard Wake

$$\epsilon_{c_F} = 1/4\ \frac{C_{D_p} \cdot S}{A\beta^3}$$

CLASSIFICATION cancelled

Model

$c_{mean} = .958'$

$t_{mean} = .144'$

$A = 195 \text{ Ft.}^2$

$A^{\frac{3}{2}} = 2730 \text{ Ft.}^3$

$s = \frac{b}{2} = 4.40'$

$\ell = 5.79'$

$d^2_{mean} = .675 \text{ Ft.}^2$

$S = 8.42 \text{ Ft.}^2$

Front Guards:

$t = .416'$

$c = 3.12'$

$\frac{t}{c} = .134$

$S = 2\left[(h \cdot c) + (c_3 \cdot \ell_3)\right] = 43.1 \text{ Ft.}^2$

Rear Guards:

$t = .375'$

$c = 2.35'$

$\ell = 6.71'$

$\frac{t}{c} = .160$

$S = c \cdot \ell + \frac{2 \cdot 50 \cdot 6.5}{144} = 20.3 \text{ Ft.}^2$

Struts:

$t_{mean} = .079'$

$c_{mean} = .813'$

$\frac{t}{c} = .097$

$\left(\frac{H}{2} - h\right) = 2.27'$

Front Struts and Strut Guards Solid Blocking,

1. Solid Blocking of Guards, $\epsilon_{c_{c'}}$

$$\Delta u_{A_1} = \frac{\Sigma g g}{4\pi}\left(\frac{1}{f^2+g^2}\right)\left\{\frac{\left(\frac{H}{2}+h\right)}{\sqrt{f^2+g^2+\left(\frac{H}{2}+h\right)^2}} - \frac{\left(\frac{H}{2}-h\right)}{\sqrt{f^2+g^2+\left(\frac{H}{2}-h\right)^2}}\right\}$$

A is at center of tunnel

$f = 1.92'$

$\frac{H}{2} = 7.76'$

$h = 5.49'$

$t = .416'$

$c = 3.12'$

$\frac{t}{c} = .134$

$\left.\begin{aligned} \frac{g}{c} &= .480 \\ \frac{q}{Ut} &= 1.09 \end{aligned}\right\}$ Figure 4, Shape B, Reference 1

$g^2 = c^2\left(\frac{g}{c}\right)^2 = 2.24 \text{ Ft.}^2$

$qg = Utc\left(\frac{q}{Ut}\right)\left(\frac{g}{c}\right) = .523\ Utc$

$\leqq qg = 2\ qg$ For Shape B

$= 1.046\ Utc$

$$\Delta u_{A_1} = \frac{1.046\ Utc}{4\pi}\left(\frac{1}{3.69 + 2.24}\right)\left\{\frac{7.76 + 5.49}{\sqrt{3.69 + 2.24 + 175.6}} - \frac{7.76 - 5.49}{\sqrt{3.69 + 2.24 + 5.15}}\right\}$$

$\Delta u_{A_1} = .00424\ Utc$ (1 guard)

$\epsilon_{c_1} = \frac{\Delta u_{A_1}}{U} = .00848\ tc$ (2 guards)

$\epsilon_{c_{c1}} = \frac{.00848\ tc}{\beta^3}$

$\epsilon_{c_{c1}} = \frac{.0110}{\beta^3}$

2. Solid Blocking of Struts, $\epsilon_{c_{c2}}$

$$\Delta u_{A_2} = \frac{\Sigma qg}{4\pi}\left(\frac{1}{f^2+g^2}\right)\left\{\frac{\left(\frac{H}{2}-h\right)}{\sqrt{f^2+g^2+\left(\frac{H}{2}-h\right)^2}}\right\}$$

A is at center of tunnel

$f = 1.92'$

$\frac{H}{2} = 7.76'$

$h = 5.49'$

$t = .079$

$c = .813'$

$\frac{t}{c} = .097$

$\frac{g}{c} = .485$

$\frac{q}{Ut} = 1.04$

Figure 4, Shape B, Reference 1

$g^2 = c^2 \left(\frac{g}{c}\right)^2 = .155 \text{ Ft.}^2$

$qg = Utc \left(\frac{q}{Ut}\right)\left(\frac{g}{c}\right) = .505 \, Utc$

$\leqslant qg = 2 \, qg$ for shape B

$= 1.010 \, Utc$

$$\Delta u_{A_2} = \frac{1.010 \, Utc}{4\pi} \left(\frac{1}{3.69 + .16}\right) \left\{\frac{2.27}{\sqrt{3.69 + .16 + 5.15}}\right\}$$

$$\Delta u_{A_2} = .0158 \, Utc \text{ (1 strut)}$$

$$\epsilon_{c_2} = \frac{\Delta u_{A_2}}{U} = .0316 \, tc \text{ (2 struts)}$$

$$\epsilon_{c_{c2}} = \frac{.0316 \, tc}{\beta^5}$$

$$\epsilon_{c_{c2}} = \frac{.0020}{\beta^3}$$

Table I - Model Parasite Drag, C_{D_p}

M	$C_L = 0$			$C_L = .1$			$C_L = .2$			$C_L = .3$			$C_L = .4$			$C_L = .5$		
	C_D	$\frac{C_L^2}{\pi AR}$	C_{D_p}	C_D	$\frac{C_L^2}{\pi AR}$	C_{D_p}	C_D	$\frac{C_L^2}{\pi AR}$	C_{D_p}	C_D	$\frac{C_L^2}{\pi AR}$	C_{D_p}	C_D	$\frac{C_L^2}{\pi AR}$	C_{D_p}	C_D	$\frac{C_L^2}{\pi AR}$	C_{D_p}
.3	.0227	0	.0227	.0215	.0003	.0212	.0219	.0014	.0205	.0234	.0031	.0203	.0256	.0052	.0204	.0288	.0087	.0201
.5	.0241		.0241	.0228		.0225	.0235		.0221	.0253		.0222	.0274		.0222	.0299		.0212
.6	.0256		.0256	.0239		.0236	.0239		.0225	.0253		.0222	.0275		.0223	.0306		.0219
.65	.0271		.0271	.0259		.0256	.0255		.0241	.0264		.0233	.0292		.0240	.0348		.0261
.675	.0304		.0304	.0279		.0276	.0273		.0259	.0287		.0256	.0346		.0294	.0500		.0413
.7	.0380		.0380	.0368		.0365	.0380		.0366	.0443		.0412	.0603		.0551	.0920		.0833
.725	.0554		.0554	.0523		.0520	.0563		.0549	.0730		.0699	.0940		.0888	.1245		.1158
.74	.0738		.0733	.0711		.0708	.0801		.0787	.0952		.0921	.1182		.1130	--	--	--
.75	.0947		.0947	.0929		.0926	.1018		.1004	.1235		.1204	.1440		.1388	--	--	--

$$C_{D_p} = C_D - \frac{C_L^2}{\pi AR} \; ; \qquad AR = 9.19$$

CLASSIFICATION cancelled

CLASSIFICATION cancelled

Table II - Model Wake Blocking, ϵ_{c_D}/β^3

M	$C_L = 0$ ϵ_{c_D}/β^3	$C_L = .1$ ϵ_{c_D}/β^3	$C_L = .2$ ϵ_{c_D}/β^3	$C_L = .3$ ϵ_{c_D}/β^3	$C_L = .4$ ϵ_{c_D}/β^3	$C_L = .5$ ϵ_{c_D}/β^3
.3	.0002	.0002	.0002	.0002	.0002	.0002
.5	.0003	.0002	.0002	.0002	.0002	.0002
.6	.0003	.0003	.0002	.0002	.0002	.0002
.65	.0003	.0003	.0003	.0003	.0003	.0003
.675	.0003	.0003	.0003	.0003	.0003	.0004
.7	.0004	.0004	.0004	.0004	.0006	.0009
.725	.0006	.0006	.0006	.0008	.0010	.0013
.74	.0008	.0008	.0009	.0010	.0012	---
.75	.0010	.0010	.0011	.0013	.0015	---

$$\epsilon_{c_D} = \frac{.0108\ C_{D_P}}{\beta^3}$$

CONFIDENTIAL
CLASSIFICATION cancelled

Table III - Front Guards Wake Blocking; ϵ_{c_E}/β^3

M	$\frac{M}{M_{cr}}$	$\frac{C_{Dp}}{C_{Dp_{INC}}}$	C_{D_p}	$(C_{Dp}\,S)_{SG}$	ϵ_{c_E}/β^3
.3	.422	1.00	.0065	.280	.0004
.5	.705	1.00	.0065	.280	.0004
.6	.845	1.12	.0073	.315	.0004
.65	.915	1.25	.0081	.349	.0004
.675	.950	1.35	.0088	.380	.0005
.7	.986	1.45	.0094	.405	.0005
.725	1.021	1.60	.0104	.449	.0006
.74	1.041	1.75	.0114	.491	.0006
.75	1.056	1.90	.0124	.535	.0007

$$\epsilon_{c_E} = \frac{(C_{Dp}\,S)_{SG}}{4A\beta^3}$$

$S = 43.1$ Ft.^{2}
$A = 195$ Ft.^{2}
$M_{cr} = .71$

$C_{D_{P_{INC.}}} = .0065$

$\left(\frac{C_{Dp}}{C_{Dp_{INC}}}\right)$ is from Figure 1, Appendix I, Curve a

CLASSIFICATION cancelled

Table IV - Rear Guard Wake Blocking, $\epsilon_{C_F}\beta^3$

M	$\frac{M}{M_{cr}}$	$\frac{C_{D_P}}{C_{D_{P_{INC}}}}$	C_{D_P}	$(C_{D_P} S)_{SG}$	$\epsilon_{C_F}\beta^3$
.3	.435	1.00	.0070	.142	.0002
.5	.725	1.00	.0070	.142	.0002
.6	.870	1.16	.0081	.164	.0002
.65	.942	1.32	.0092	.187	.0002
.675	.978	1.42	.0099	.201	.0003
.7	1.014	1.55	.0108	.219	.0003
.725	1.050	1.83	.0128	.260	.0003
.74	1.072	2.12	.0148	.300	.0004
.75	1.088	2.40	.0168	.341	.0004

$$\epsilon_{C_F} = \frac{(C_{D_P} S)_{SG}}{4A\beta^3}$$

$S = 20.3$ Ft.^{2}
$A = 195$
$M_{cr} = .69$

$C_{D_{P_{INC}}} = .0070$

$\left(\frac{C_{D_P}}{C_{D_{P_{INC}}}}\right)$ is from Figure 1, Appendix I, Curve a.

CLASSIFICATION cancelled

CLASSIFICATION cancelled

Table V - $(\epsilon_{c_A}+\epsilon_{c_C}+\epsilon_{c_D}+\epsilon_{c_E}+\epsilon_{c_F})_1$ AND $(\epsilon_{c_B})_1$

M	$\frac{1}{\beta^3}$	$(\epsilon_{c_A}+\epsilon_{c_C}+\epsilon_{c_D}+\epsilon_{c_E}+\epsilon_{c_F})\beta^3$						$(\epsilon_{c_A}+\epsilon_{c_C}+\epsilon_{c_D}+\epsilon_{c_E}+\epsilon_{c_F})_1$						$\frac{1}{\beta^4}$	$\epsilon_{c_B}\beta^4$	$(\epsilon_{c_B})_1$
		$C_L=0$	$C_L=.1$	$C_L=.2$	$C_L=.3$	$C_L=.4$	$C_L=.5$	$C_L=0$	$C_L=.1$	$C_L=.2$	$C_L=.3$	$C_L=.4$	$C_L=.5$			
.3	1.16	.0141	.0141	.0141	.0141	.0141	.0141	.0164	.0164	.0164	.0164	.0164	.0164	1.21	.0006	.0007
.5	1.54	.0142	.0141	.0141	.0141	.0141	.0141	.0218	.0217	.0217	.0217	.0217	.0217	1.78		.0011
.6	1.90	.0142	.0142	.0141	.0141	.0141	.0141	.0270	.0270	.0268	.0268	.0268	.0268	2.44		.0015
.65	2.28	.0142	.0142	.0142	.0142	.0142	.0142	.0324	.0324	.0324	.0324	.0324	.0324	3.00		.0018
.675	2.49	.0144	.0144	.0144	.0144	.0144	.0145	.0358	.0358	.0358	.0358	.0358	.0361	3.35		.0020
.7	2.75	.0145	.0145	.0145	.0145	.0147	.0150	.0399	.0399	.0399	.0399	.0404	.0412	3.85		.0023
.725	3.05	.0148	.0148	.0148	.0150	.0152	.0155	.0451	.0451	.0451	.0457	.0463	.0472	4.45		.0027
.74	3.29	.0151	.0151	.0152	.0153	.0155	--	.0496	.0496	.0500	.0503	.0510	--	4.88		.0029
.75	3.45	.0154	.0154	.0155	.0157	.0159	--	.0531	.0531	.0534	.0541	.0548	--	5.23		.0031

$\frac{1}{\beta^3}$ and $\frac{1}{\beta^4}$ are from Figure 1

CLASSIFICATION cancelled

CLASSIFICATION cancelled

Table VI, $(\Sigma \epsilon_c)_1$

M	$(\Sigma \epsilon_c)_1$					
	$C_L=0$	$C_L=.1$	$C_L=.2$	$C_L=.3$	$C_L=.4$	$C_L=.5$
.3	.0171	.0171	.0171	.0171	.0171	.0171
.5	.0229	.0228	.0228	.0228	.0228	.0228
.6	.0285	.0285	.0283	.0283	.0283	.0283
.65	.0342	.0342	.0342	.0342	.0342	.0342
.675	.0378	.0378	.0378	.0378	.0378	.0381
.7	.0422	.0422	.0422	.0422	.0427	.0435
.725	.0478	.0478	.0478	.0484	.0490	.0499
.74	.0525	.0525	.0529	.0532	.0539	---
.75	.0562	.0562	.0565	.0572	.0579	---

$$(\Sigma \epsilon_c)_1 = (\epsilon_{c_A} + \epsilon_{c_B} + \epsilon_{c_C} + \epsilon_{c_D} + \epsilon_{c_E} + \epsilon_{c_F})_1$$

CLASSIFICATION cancelled

CLASSIFICATION cancelled

Table VII - First Approximation of Corrected Mach Number, M_{c_1}

M	M^2	$1+\frac{\gamma-1}{2}M^2$	$C_L = 0$		$C_L = .1$		$C_L = .2$		$C_L = .3$		$C_L = .4$		$C_L = .5$	
			$(\Sigma\epsilon_d)_1(1+\frac{\gamma-1}{2}M^2)$	M_{c_1}	$(\Sigma\epsilon_d)_1(1+\frac{\gamma-1}{2}M^2)$	M_{c_1}	$(\Sigma\epsilon_d)_1(1+\frac{\gamma-1}{2}M^2)$	M_{c_1}	$(\Sigma\epsilon_d)_1(1+\frac{\gamma-1}{2}M^2)$	M_{c_1}	$(\Sigma\epsilon_d)_1(1+\frac{\gamma-1}{2}M^2)$	M_{c_1}	$(\Sigma\epsilon_d)_1(1+\frac{\gamma-1}{2}M^2)$	M_{c_1}
.3	.090	1.018	.0174	.305	.0174	.305	.0174	.305	.0174	.305	.0174	.305	.0174	.305
.5	.250	1.050	.0240	.512	.0239	.512	.0239	.512	.0239	.512	.0239	.512	.0239	.512
.6	.360	1.072	.0306	.619	.0306	.619	.0304	.619	.0304	.619	.0304	.619	.0304	.619
.65	.422	1.084	.0371	.674	.0371	.674	.0371	.674	.0371	.674	.0371	.674	.0371	.674
.675	.456	1.091	.0412	.703	.0412	.703	.0412	.703	.0412	.703	.0412	.703	.0416	.703
.7	.490	1.098	.0463	.731	.0463	.731	.0463	.731	.0463	.731	.0469	.732	.0477	.732
.725	.526	1.105	.0528	.764	.0528	.764	.0528	.764	.0535	.764	.0541	.764	.0551	.765
.74	.548	1.110	.0583	.781	.0583	.781	.0587	.781	.0591	.782	.0598	.783	--	--
.75	.563	1.113	.0625	.797	.0625	.797	.0629	.798	.0637	.798	.0644	.799	--	--

$$M_{c_1} = M\left[1+(\Sigma\epsilon_d)_1\left(1+\frac{\gamma-1}{2}M^2\right)\right]$$

$(\Sigma\epsilon_d)_1$ is from Table VI

CLASSIFICATION cancelled

CLASSIFICATION cancelled

Table VIII - $(\epsilon_{c_A} + \epsilon_{c_C} + \epsilon_{c_D} + \epsilon_{c_E} + \epsilon_{c_F})$ AND (ϵ_{c_B})

M	M_{AV}	$\frac{1}{\beta^3}$	$(\epsilon_{c_A} + \epsilon_{c_C} + \epsilon_{c_D} + \epsilon_{c_E} + \epsilon_{c_F})\beta^3$						$(\epsilon_{c_A} + \epsilon_{c_C} + \epsilon_{c_D} + \epsilon_{c_E} + \epsilon_{c_F})$						$\frac{1}{\beta^4}$	$\epsilon_{c_B}\beta^4$	ϵ_{c_B}
			$C_L=0$	$C_L=.1$	$C_L=.2$	$C_L=.3$	$C_L=.4$	$C_L=.5$	$C_L=0$	$C_L=.1$	$C_L=.2$	$C_L=.3$	$C_L=.4$	$C_L=.5$			
.3	.303	1.16	.0141	.0141	.0141	.0141	.0141	.0141	.0164	.0164	.0164	.0164	.0164	.0164	1.21	.0006	.0007
.5	.506	1.56	.0142	.0141	.0141	.0141	.0141	.0141	.0222	.0220	.0220	.0220	.0220	.0220	1.81		.0011
.6	.610	2.00	.0142	.0142	.0141	.0141	.0141	.0141	.0284	.0284	.0282	.0282	.0282	.0282	2.53		.0015
.65	.662	2.37	.0142	.0142	.0142	.0142	.0142	.0142	.0336	.0336	.0336	.0336	.0336	.0336	3.15		.0019
.675	.689	2.61	.0144	.0144	.0144	.0144	.0144	.0145	.0376	.0376	.0376	.0376	.0376	.0378	3.60		.0022
.7	.716	2.94	.0145	.0145	.0145	.0145	.0147	.0150	.0426	.0426	.0426	.0426	.0432	.0441	4.21		.0025
.725	.745	3.35	.0148	.0148	.0148	.0150	.0152	.0155	.0495	.0495	.0495	.0502	.0509	.0519	5.03		.0030
.74	.762	3.65	.0151	.0151	.0152	.0153	.0155	--	.0551	.0551	.0555	.0558	.0565	--	5.66		.0034
.75	.774	3.90	.0154	.0154	.0155	.0157	.0159	--	.0600	.0600	.0604	.0611	.0620	--	6.19		.0037

$M_{AV} = \frac{M + M_{C_L}}{2}$ $\quad M_{C_L}$ from Table VII

$\frac{1}{\beta^3}$ AND $\frac{1}{\beta^4}$ are from Figure 1 using M_{AV} in place of M.

CLASSIFICATION cancelled

CONFIDENTIAL
CLASSIFICATION cancelled

Table IX, $\Sigma \epsilon_c$

M	$\Sigma \epsilon_c$					
	$C_L = 0$	$C_L = .1$	$C_L = .2$	$C_L = .3$	$C_L = .4$	$C_L = .5$
.3	.0171	.0171	.0171	.0171	.0171	.0171
.5	.0233	.0231	.0231	.0231	.0231	.0231
.6	.0299	.0299	.0297	.0297	.0297	.0297
.65	.0355	.0355	.0355	.0355	.0355	.0355
.675	.0398	.0398	.0398	.0398	.0398	.0400
.7	.0451	.0451	.0451	.0451	.0457	.0466
.725	.0525	.0525	.0525	.0532	.0539	.0549
.74	.0585	.0585	.0589	.0592	.0599	---
.75	.0637	.0637	.0641	.0648	.0657	---

$$\Sigma \epsilon_c = \left(\epsilon_{c_A} + \epsilon_{c_B} + \epsilon_{c_C} + \epsilon_{c_D} + \epsilon_{c_E} + \epsilon_{c_F} \right)$$

CLASSIFICATION cancelled
CONFIDENTIAL

CLASSIFICATION cancelled

Table X-Corrected Mach Number, M_c

M	M_{AV}	M_{AV}^2	$1+\frac{\gamma-1}{2}M_{AV}^2$	$C_L=0$		$C_L=.1$		$C_L=.2$		$C_L=.3$		$C_L=.4$		$C_L=.5$	
				$\Sigma\epsilon_c\left(1+\frac{\gamma-1}{2}M_{AV}^2\right)$	M_c	$\Sigma\epsilon_c\left(1+\frac{\gamma-1}{2}M_{AV}^2\right)$	M_c	$\Sigma\epsilon_c\left(1+\frac{\gamma-1}{2}M_{AV}^2\right)$	M_c	$\Sigma\epsilon_c\left(1+\frac{\gamma-1}{2}M_{AV}^2\right)$	M_c	$\Sigma\epsilon_c\left(1+\frac{\gamma-1}{2}M_{AV}^2\right)$	M_c	$\Sigma\epsilon_c\left(1+\frac{\gamma-1}{2}M_{AV}^2\right)$	M_c
.3	.303	.092	1.018	.0174	.305	.0174	.305	.0174	.305	.0174	.305	.0174	.305	.0174	.305
.5	.506	.256	1.051	.0245	.513	.0243	.513	.0243	.513	.0243	.513	.0243	.513	.0243	.513
.6	.610	.372	1.074	.0321	.620	.0321	.620	.0319	.620	.0319	.620	.0319	.620	.0319	.620
.65	.662	.438	1.088	.0386	.675	.0386	.675	.0386	.675	.0386	.675	.0386	.675	.0386	.675
.675	.684	.474	1.095	.0436	.705	.0436	.705	.0436	.705	.0436	.705	.0436	.705	.0438	.705
.7	.716	.513	1.103	.0498	.735	.0498	.735	.0498	.735	.0498	.735	.0505	.735	.0515	.736
.725	.745	.555	1.111	.0583	.766	.0583	.766	.0583	.766	.0591	.767	.0599	.768	.0610	.769
.74	.762	.581	1.116	.0653	.788	.0653	.788	.0657	.789	.0661	.789	.0668	.789	--	--
.75	.774	.599	1.120	.0714	.804	.0714	.804	.0718	.804	.0725	.805	.0736	.805	--	--

$$M_c = M\left[1+\Sigma\epsilon_c\left(1+\frac{\gamma-1}{2}M_{AV}^2\right)\right]$$

$\Sigma\epsilon_c$ is from Table IX

CLASSIFICATION cancelled

CLASSIFICATION cancelled

Table XI, $(M_c - M)$

M	$(M_c - M)$					
	$C_L = 0$	$C_L = .1$	$C_L = .2$	$C_L = .3$	$C_L = .4$	$C_L = .5$
.3	.005	.005	.005	.005	.005	.005
.5	.013	.013	.013	.013	.013	.013
.6	.020	.020	.020	.020	.020	.020
.65	.025	.025	.025	.025	.025	.025
.675	.030	.030	.030	.030	.030	.030
.7	.035	.035	.035	.035	.035	.036
.725	.041	.041	.041	.042	.043	.044
.74	.048	.048	.049	.049	.049	---
.75	.054	.054	.054	.055	.055	---

CLASSIFICATION cancelled

CONFIDENTIAL

CLASSIFICATION cancelled

Table XII-Corrected Drag Coefficient, C_{D_c}

M	M^2	$(2-M^2)$	$C_L = 0$				$C_L = .1$				$C_L = .2$			
			$\Sigma\epsilon_c$	$\Sigma\epsilon_c(2-M^2)$	C_D	C_{D_c}	$\Sigma\epsilon_c$	$\Sigma\epsilon_c(2-M^2)$	C_D	C_{D_c}	$\Sigma\epsilon_c$	$\Sigma\epsilon_c(2-M^2)$	C_D	C_{D_c}
.3	.090	1.910	.0171	.0326	.0227	.0220	.0171	.0326	.0215	.0208	.0171	.0326	.0219	.0212
.5	.250	1.750	.0233	.0408	.0241	.0231	.0231	.0404	.0228	.0219	.0231	.0404	.0235	.0225
.6	.360	1.640	.0299	.0490	.0256	.0244	.0299	.0490	.0239	.0227	.0297	.0487	.0239	.0227
.65	.422	1.578	.0355	.0560	.0271	.0256	.0355	.0560	.0259	.0244	.0355	.0560	.0255	.0241
.675	.456	1.544	.0398	.0615	.0304	.0285	.0398	.0615	.0279	.0262	.0398	.0615	.0273	.0256
.7	.490	1.510	.0451	.0681	.0380	.0354	.0451	.0681	.0368	.0343	.0451	.0681	.0380	.0354
.725	.526	1.474	.0525	.0774	.0554	.0511	.0525	.0774	.0523	.0482	.0525	.0774	.0563	.0519
.74	.548	1.452	.0585	.0850	.0738	.0675	.0585	.0850	.0711	.0651	.0589	.0855	.0801	.0738
.75	.563	1.437	.0637	.0915	.0947	.0860	.0637	.0915	.0929	.0844	.0641	.0921	.1018	.0924

CONFIDENTIAL
CLASSIFICATION cancelled

CONFIDENTIAL
CLASSIFICATION cancelled

Table XII (Continued)

M	M^2	$(2-M^2)$	$C_L = .3$				$C_L = .4$				$C_L = .5$			
			$\Sigma\epsilon_c$	$\Sigma\epsilon_c(2-M^2)$	C_D	C_{D_c}	$\Sigma\epsilon_c$	$\Sigma\epsilon_c(2-M^2)$	C_D	C_{D_c}	$\Sigma\epsilon_c$	$\Sigma\epsilon_c(2-M^2)$	C_D	C_{D_c}
.3	.090	1.910	.0171	.0326	.0234	.0226	.0171	.0326	.0256	.0248	.0171	.0326	.0288	.0278
.5	.250	1.750	.0231	.0404	.0253	.0243	.0231	.0404	.0274	.0263	.0231	.0404	.0299	.0287
.6	.360	1.640	.0297	.0487	.0253	.0241	.0247	.0487	.0275	.0262	.0297	.0487	.0306	.0291
.65	.422	1.578	.0355	.0560	.0264	.0249	.0355	.0560	.0292	.0276	.0355	.0560	.0348	.0328
.675	.456	1.544	.0398	.0615	.0287	.0269	.0398	.0615	.0346	.0325	.0400	.0618	.0500	.0469
.7	.490	1.510	.0451	.0681	.0443	.0413	.0457	.0690	.0603	.0561	.0466	.0704	.0920	.0855
.725	.526	1.474	.0532	.0785	.0730	.0673	.0539	.0794	.0940	.0865	.0549	.0809	.1245	.1143
.74	.548	1.452	.0592	.0860	.0952	.0870	.0599	.0870	.1182	.1080	--	--	--	--
.75	.563	1.437	.0648	.0930	.1235	.1120	.0657	.0944	.1440	.1304	--	--	--	--

$$C_{D_c} = C_D \left[1 - \Sigma\epsilon_c(2-M^2) \right]$$

$\Sigma\epsilon_c$ is from Table IX

CLASSIFICATION cancelled

CONFIDENTIAL
CLASSIFICATION cancelled

Table XIII-Corrected Drag Ratio, $\left(\frac{C_D}{C_{D_{INC}}}\right)_c$

M	$C_L=0;\ (C_{D_{INC}})_c=.0220$		$C_L=.1;\ (C_{D_{INC}})_c=.0208$		$C_L=.2;\ (C_{D_{INC}})_c=.0212$		$C_L=.3;\ (C_{D_{INC}})_c=.0226$		$C_L=.4;\ (C_{D_{INC}})_c=.0248$		$C_L=.5;\ (C_{D_{INC}})_c=.0278$	
	C_{D_c}	$\left(\frac{C_D}{C_{D_{INC}}}\right)_c$	C_{D_c}	$\left(\frac{C_D}{C_{D_{INC}}}\right)_c$	C_{D_c}	$\left(\frac{C_D}{C_{D_{INC}}}\right)_c$	C_{D_c}	$\left(\frac{C_D}{C_{D_{INC}}}\right)_c$	C_{D_c}	$\left(\frac{C_D}{C_{D_{INC}}}\right)_c$	C_{D_c}	$\left(\frac{C_D}{C_{D_{INC}}}\right)_c$
.3	.0220	1.000	.0208	1.000	.0212	1.000	.0226	1.000	.0248	1.000	.0278	1.000
.5	.0231	1.050	.0219	1.052	.0225	1.061	.0243	1.075	.0263	1.060	.0287	1.032
.6	.0244	1.109	.0227	1.901	.0227	1.071	.0241	1.068	.0262	1.056	.0291	1.047
.65	.0256	1.163	.0244	1.173	.0241	1.138	.0249	1.102	.0276	1.112	.0328	1.180
.675	.0285	1.296	.0262	1.260	.0256	1.208	.0269	1.190	.0325	1.310	.0469	1.687
.7	.0354	1.610	.0343	1.650	.0354	1.670	.0413	1.829	.0561	2.26	.0855	3.08
.725	.0511	2.33	.0482	2.32	.0519	2.45	.0673	2.98	.0865	3.49	.1143	4.11
.74	.0675	3.07	.0651	3.13	.0738	3.48	.0870	3.85	.1080	4.36	--	--
.75	.0860	3.91	.0844	4.06	.0924	4.38	.1120	4.96	.1304	5.26	--	--

C_{D_c} is from Table XII

$(C_{D_{INC}})_c = C_{D_c}$ AT $M=.3$

CLASSIFICATION CONFIDENTIAL cancelled

CONFIDENTIAL
CLASSIFICATION cancelled

Table XIV-Mach Number Ratio, $\left(\frac{M}{M_{cr}}\right)_c$

M	$C_L = 0$ $(M_{cr})_c = .632$		$C_L = .1$ $(M_{cr})_c = .625$		$C_L = .2$ $(M_{cr})_c = .607$		$C_L = .3$ $(M_{cr})_c = .583$		$C_L = .4$ $(M_{cr})_c = .561$		$C_L = .5$ $(M_{cr})_c = .539$	
	M_c	$\left(\frac{M}{M_{cr}}\right)_c$	M_c	$\left(\frac{M}{M_{cr}}\right)_c$	M_c	$\left(\frac{M}{M_{cr}}\right)_c$	M_c	$\left(\frac{M}{M_{cr}}\right)_c$	M_c	$\left(\frac{M}{M_{cr}}\right)_c$	M_c	$\left(\frac{M}{M_{cr}}\right)_c$
.3	.305	.482	.305	.488	.305	.502	.305	.523	.305	.544	.305	.565
.5	.513	.811	.513	.821	.513	.845	.513	.880	.513	.915	.513	.951
.6	.620	.981	.620	.991	.620	1.021	.620	1.062	.620	1.105	.620	1.150
.65	.675	1.068	.675	1.080	.675	1.111	.675	1.158	.675	1.202	.675	1.251
.675	.705	1.115	.705	1.128	.705	1.161	.705	1.209	.705	1.257	.705	1.303
.7	.735	1.162	.735	1.176	.735	1.210	.735	1.260	.735	1.310	.736	1.367
.725	.766	1.212	.766	1.227	.766	1.262	.767	1.316	.768	1.369	.769	1.425
.74	.788	1.246	.788	1.260	.789	1.299	.789	1.351	.789	1.405	--	--
.75	.804	1.270	.804	1.287	.804	1.322	.805	1.380	.805	1.435	--	--

M_c is from Table X

CLASSIFICATION cancelled
CONFIDENTIAL

CLASSIFICATION cancelled

TEST SECTION OF AAL 16 FOOT WIND TUNNEL

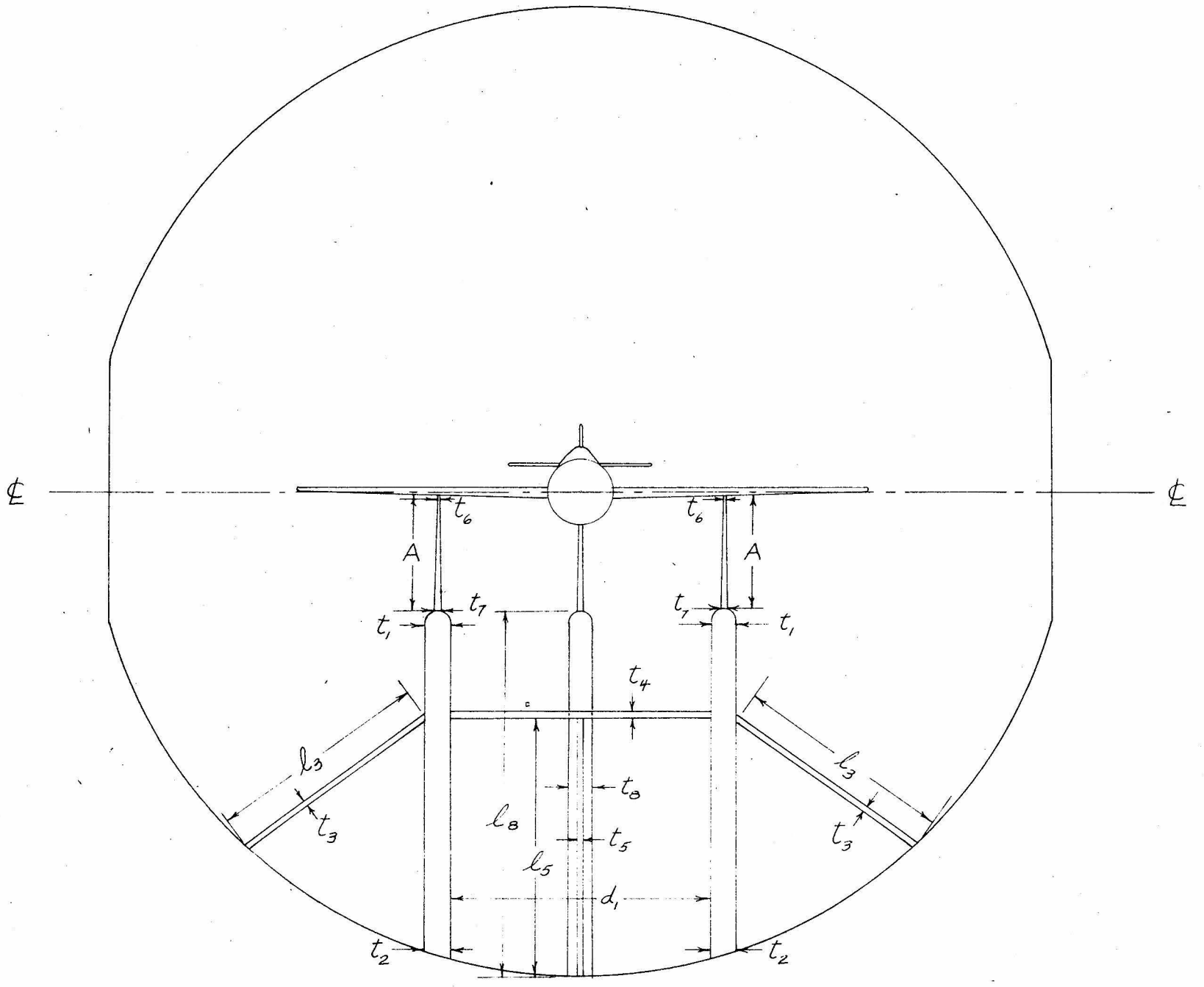

LOOKING DOWNSTREAM

TEST	METHOD OF CALIBRATION	DIMENSION (INCHES)																				
		A	d_1	t_1	t_2	t_3	t_4	t_5	t_6	t_7	t_8	C_1	C_2	C_3	C_4	C_5	C_6	C_7	C_8	l_3	l_5	l_8
B-29	TUNNEL EMPTY	12.2	73	1.5	2	.75	.75	.69	.31	.50	4.5	11.5	23.25	6	6	5	2.0	4.25	28.25	40	60	92.5
B-42	STRUTS IN	27.2	75	5	5	△1.75	NONE	NONE	.45	1.25	4.5	37.5	37.5	△13	NONE	NONE	4.5	15.0	28.25	△30	NONE	80.5
C-69	TUNNEL EMPTY	27.2	46.14	5	5	1.56	NONE	NONE	.56	1.34	4.5	37.5	37.5	13	NONE	NONE	4.5	15.0	28.25	49	NONE	80.5
P-38	TUNNEL EMPTY	28.5	27	5	5	□.375	□.375	NONE	1.00	1.60	NONE	34.0	34.0	□.375	□.375	NONE	7.75	14.5	NONE	□68.5	NONE	NONE
P-47	STRUTS IN	27.2	75	5	5	1.56	NONE	NONE	.45	1.25	4.5	37.5	37.5	13	NONE	NONE	4.5	15.0	28.25	37.5	NONE	92.5
P-51B	STRUTS IN	27.2	75	5	5	1.56	NONE	NONE	.45	1.25	4.5	37.5	37.5	13	NONE	NONE	4.5	15.0	28.25	37.5	NONE	92.5
P-58	TUNNEL EMPTY	27.2	35.67	5	5	1.56	NONE	NONE	1.00	1.57	NONE	37.5	37.5	13	NONE	NONE	7.75	14.5	NONE	54	NONE	NONE
XSB2D-1	STRUTS IN	27.2	65.85	5	5	1.56	NONE	NONE	.95	1.55	4.5	37.5	37.5	13	NONE	NONE	8.0	15.0	28.25	41	NONE	80.5

NOTES: 1. $C_1, C_2, \ldots C_8$ ARE THE CHORD LENGTHS CORRESPONDING TO $t_1, t_2, \ldots t_8$ OF ABOVE SKETCH.

2. t_8, C_8, AND l_8 ARE FOR THE REAR (TAIL) STRUT GUARD.

3. △ - SIDE BRACES ARE HORIZONTAL.

4 □ - WIRE BRACE.

5. TAIL STRUT GUARD HAD TWO BRACES OF 50 INCH LENGTH, 6.5 INCH CHORD, AND .875 INCH THICKNESS.

6. IN XP-51 TEST, FRONT STRUTS TAPERED FROM 8 INCH CHORD AT MODEL TO 60.4 INCH CHORD AT TUNNEL WALL. THEY WERE OF CONSTANT THICKNESS RATIO, 5 PER CENT, AND HAD NO GUARD OR WINDSHIELD. BOTH THE REAR STRUT AND ITS GUARD WERE 7 PER CENT THICK AND OF CONSTANT CHORD. FOR THIS TEST, THE TUNNEL WAS CALIBRATED WITH THE FRONT STRUTS IN PLACE. NO BRACING WAS USED.

TABLE XV, APPENDIX I - STRUT AND GUARD DIMENSIONS

CLASSIFICATION cancelled

RWH 9/2/44

CL CONFIDENTIAL cancelled

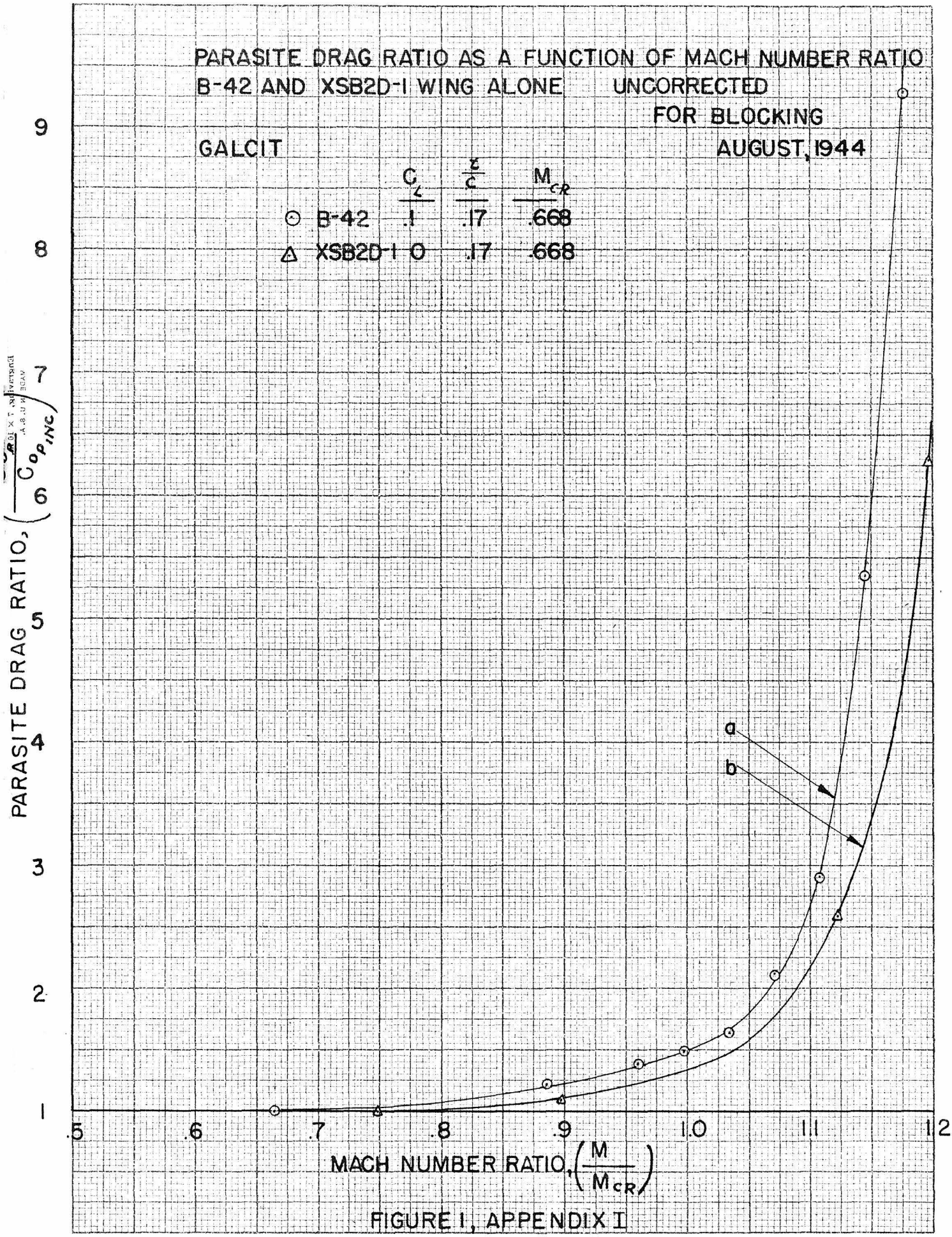

FIGURE I, APPENDIX I

CONFIDENTIAL

RWH 8/26/44

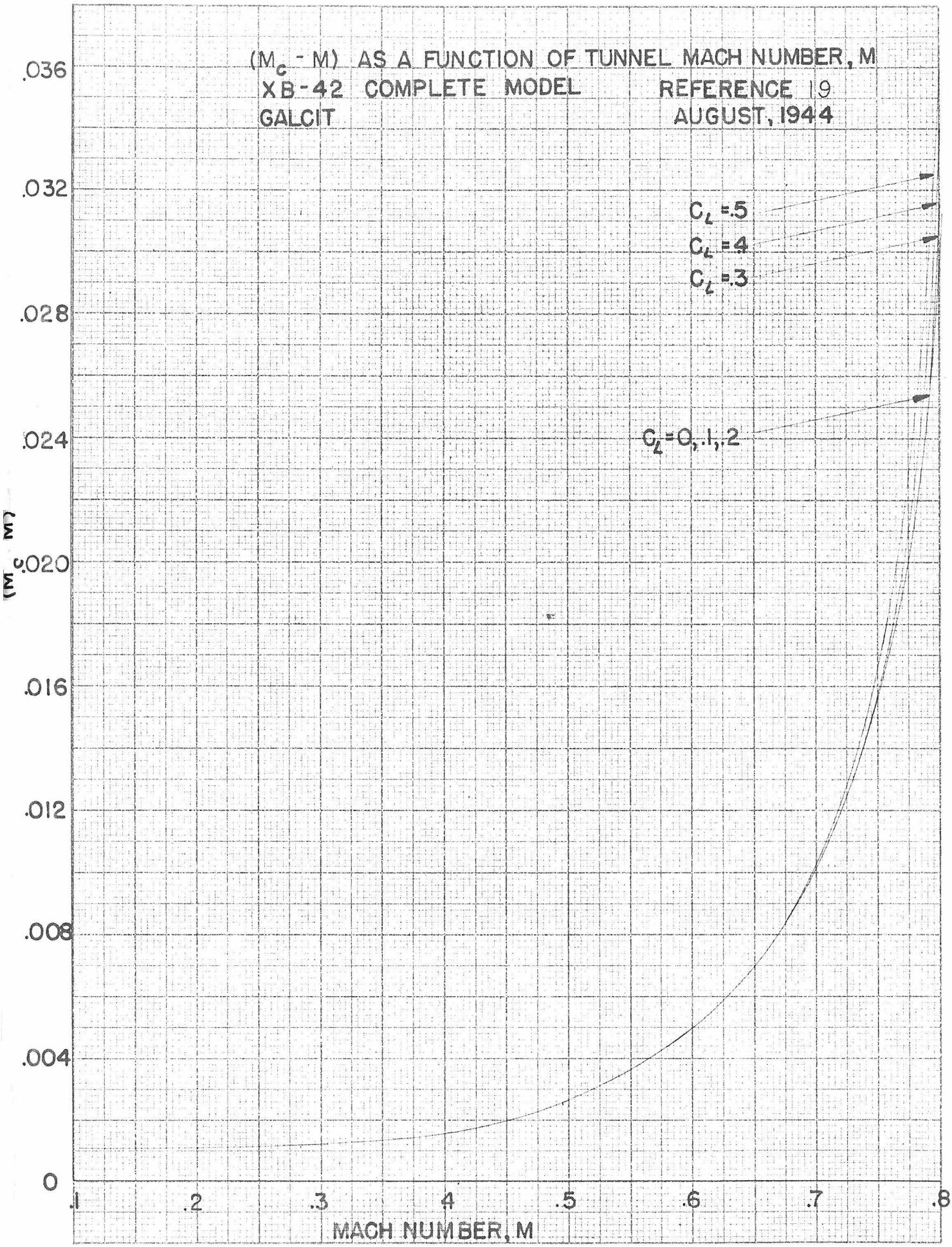

FIGURE 2, APPENDIX I

RWH 9/1144

APPENDIX II

CONFIDENTIAL cancelled

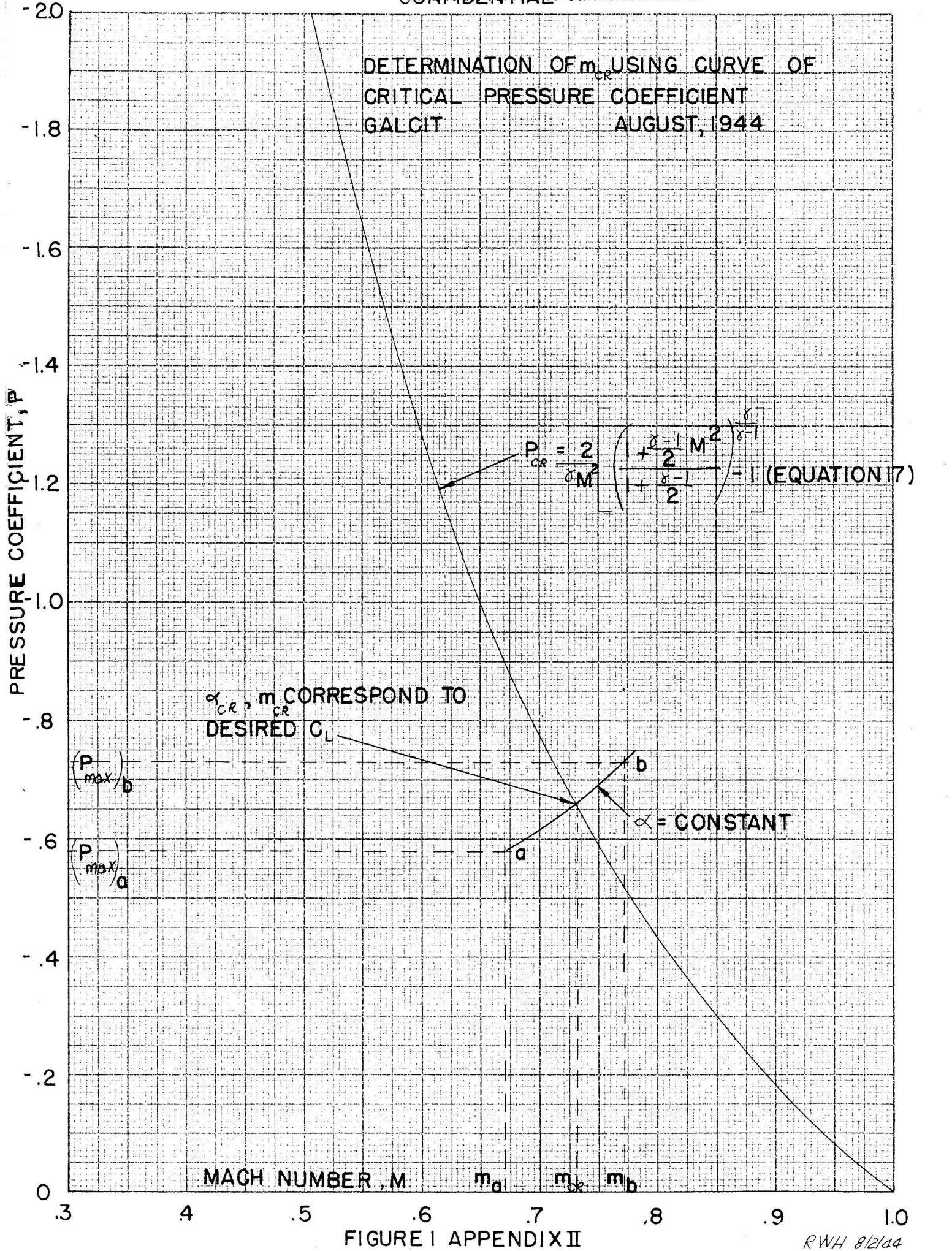

FIGURE I APPENDIX II

RWH 8/2/44

CONFIDENTIAL ON cancelled

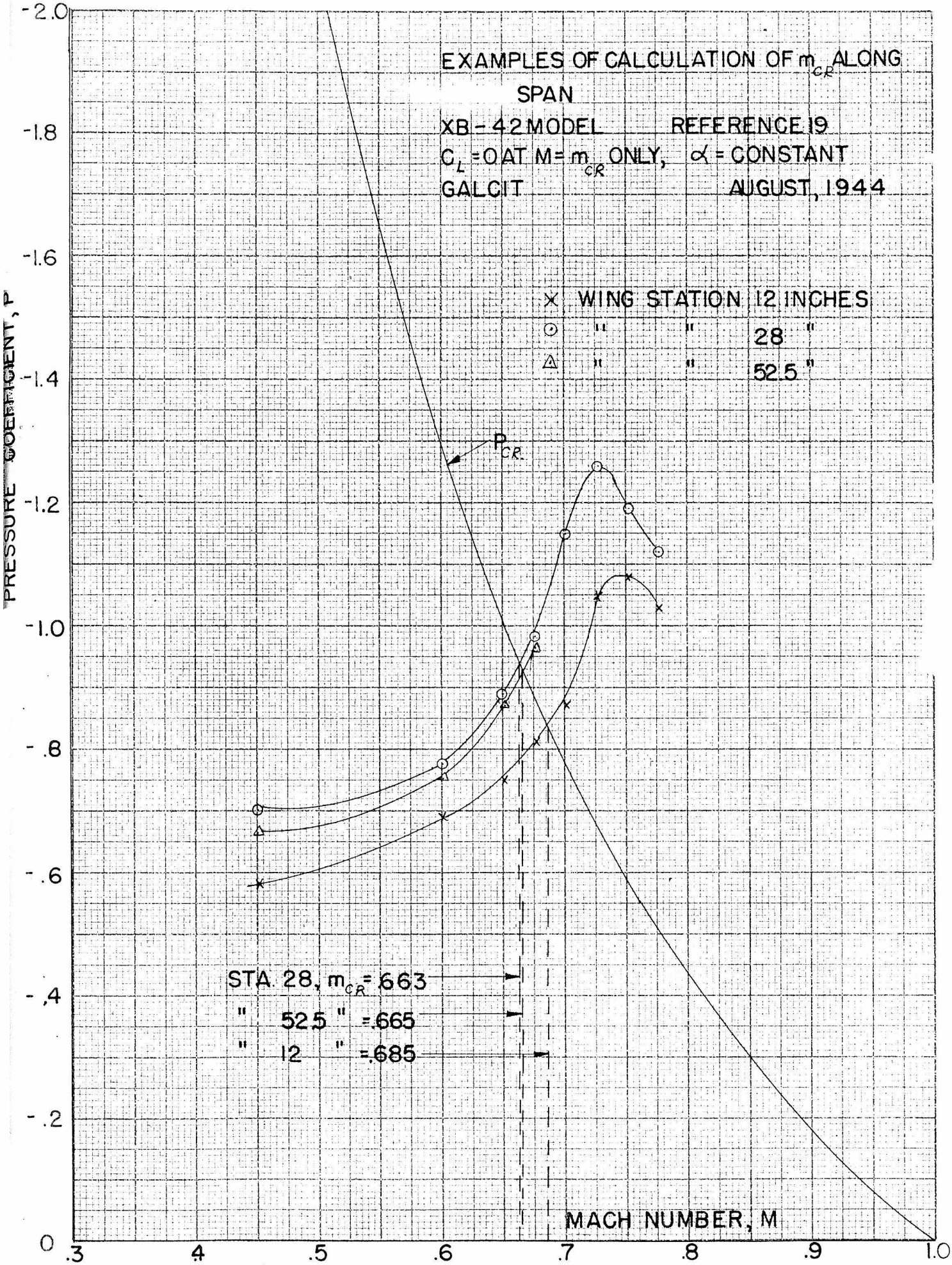

FIGURE 2 APPENDIX II

R/W/H 8/2/44

CONFIDENTIAL cancelled

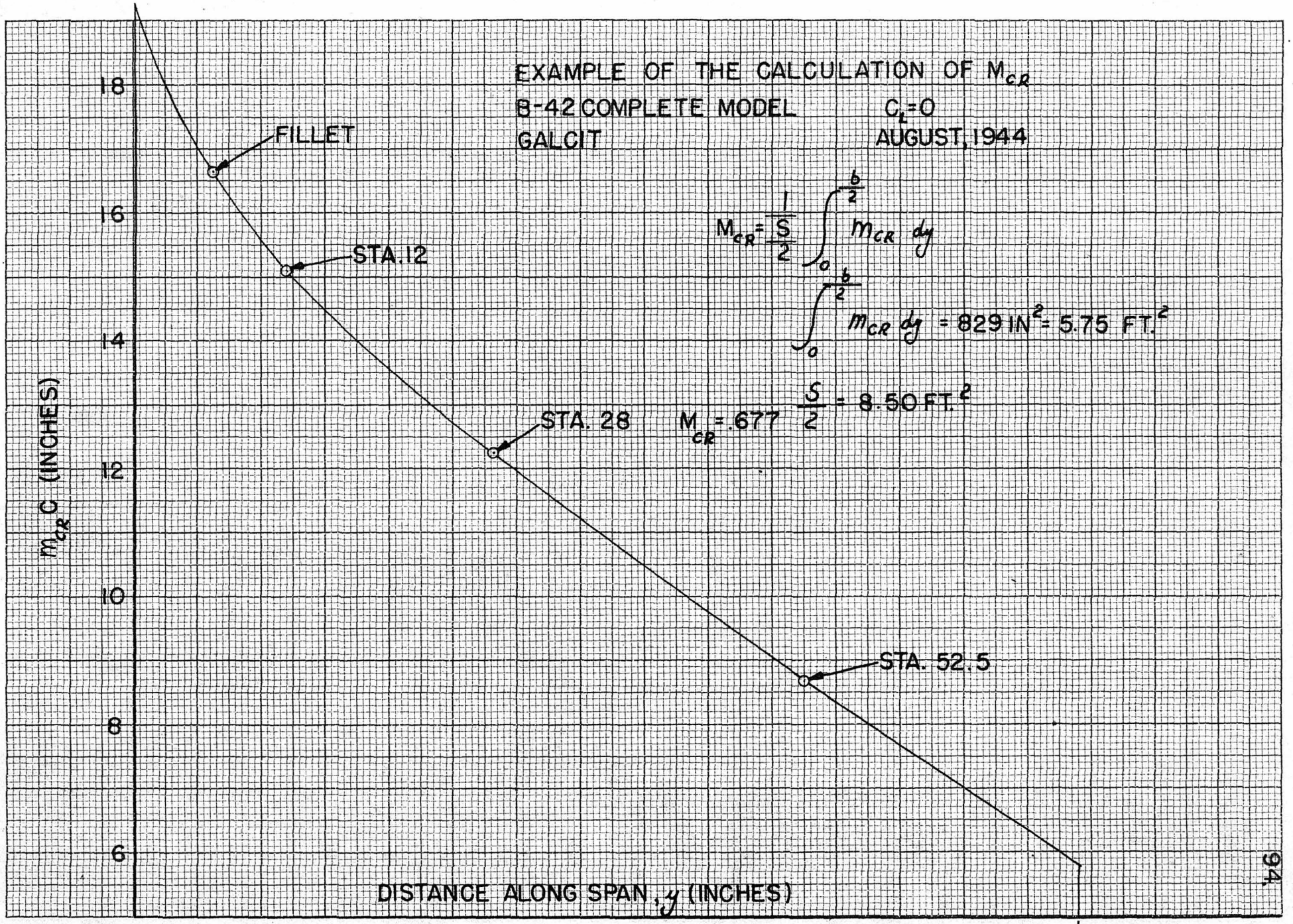

FIGURE 3, APPENDIX II

RWH 8/31/44

CONFIDENTIAL cancelled

CONFIDENTIAL
CLASSIFICATION cancelled

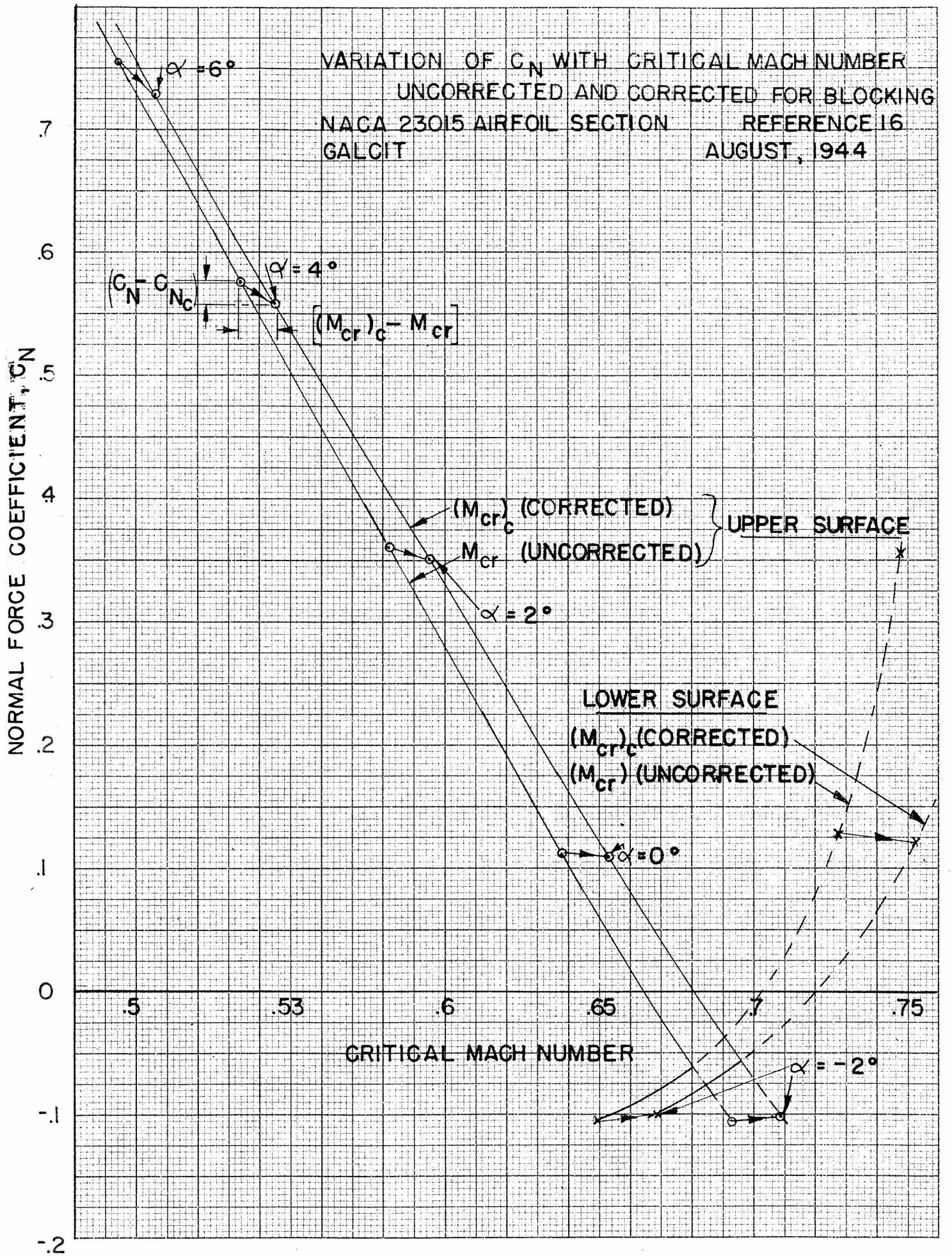

FIGURE 4 APPENDIX II